Supplementary Information

Quinoidal propylenedioxythiophene dimers for air-stable n-type semiconductors: Achieving crystallinity and solution processability

Hiroshi Nishimoto,[a] Tomoko Fujino,*[a,b] Toshiki Higashino[c] and Hatsumi Mori*[a]

[a] The Institute for Solid State Physics, The University of Tokyo, Kashiwa, Chiba 277-8581, Japan.

[b] Department of Chemistry and Life Science, Yokohama National University, Yokohama, Kanagawa, 240-8501, Japan.

[c] National Institute of Advanced Industrial Science and Technology, Tsukuba, Ibaraki 305-8565, Japan.

E-mail: fujino-tomoko-bz@ynu.ac.jp, hmori@issp.u-tokyo.ac.jp

Table of Contents

1. General

Analytical thin layer chromatography (TLC) was performed on a glass plate coated with silica gel (230–400 mesh, 0.25 mm thickness) containing a fluorescent indicator (silica gel $60F_{254}$, Merck). Gel permeation chromatography (GPC) was performed on JAIGEL-HR-40P and 2HR-40 polystyrene columns with chloroform as the eluent using a Japan Analytical Industry LaboACE LC-5060 Plus II. Proton (^{1}H) and carbon (^{13}C) nuclear magnetic resonance (NMR) spectra were recorded on a JEOL JNM-ECS400 (^{1}H NMR: 400 MHz, ^{13}C NMR: 100 MHz). The chemical shifts (δ) were referenced to tetramethylsilane ($Si(CH_3)_4$) as the internal standard (^{1}H NMR, $Si(CH_3)_4$ at 0.00 ppm; ^{13}C NMR, $Si(CH_3)_4$ at 0.00 ppm). High-resolution mass spectra (HRMS) were measured using a JEOL JMS-AX500 with a field desorption (FD) probe at the positive mode using cholesterol as an internal standard. The cyclic

voltammetry (CV) characteristics were performed using an ALS 610DB electrochemical analyzer. The CV cell consisted of a carbon working electrode, a platinum (Pt) counter electrode and a silver/silver chloride (Ag/AgCl) reference electrode. The measurements were performed in dichloromethane solution containing 0.1 M *n*-tetrabutylammonium hexafluorophosphate (n-Bu_4NPF_6) as the supporting electrolyte. Ultraviolet–visible (UV–vis) spectra were measured on JASCO V-670 spectrophotometer. Single-crystal X-ray diffraction measurements were performed using a Rigaku HyPix-6000HE (Mo $K\alpha$, λ = 0.71073 Å). UV–ozone treatment of Si/SiO_2 substrates was performed using TECHNOVISION Model208. Parylene C layer deposition onto the Si/SiO_2 substrates was performed by chemical vapor deposition using Specialty Coating Systems PDS 2010 LABCOTER. Crystalline thin films were fabricated by vacuum deposition method using Ulvac VTR-060M/ERH, blade-coating method using Opto Sigma Stepping Motor Drive SHOT-302GS, or spin-coating method using Mikasa Opticoat MS-A100. The organic field-effect transistor (OFET) properties were measured using a Keithley 4200 semiconductor characterization system and Agilent Technologies E5270A+E5270B modular source/measure units. Powder X-ray diffraction (PXRD) measurements were performed using a Rigaku SmartLab 3KW diffractometer (Cu $K\alpha$, λ = 1.5418 Å). Atomic force microscopy (AFM) images were taken in a tapping mode using a Bruker Dimension Edge.

2. Materials

Except for air oxidation to prepare **q2P** and **q2P^{Hex}**, all reactions were carried out under argon atmosphere. The following reagents were purchased from commercial suppliers: *N*-bromosuccinimide (NBS) (Wako Pure Chemical Industries), sodium hydride (60% dispersion in mineral oil, Sigma-Aldrich), malononitrile (Wako Pure Chemical Industries), tetrakis(triphenylphosphine)palladium(0) ($Pd(PPh_3)_4$) (Wako Pure Chemical Industries), 1,1′-bis(diphenylphosphino)ferrocene (dppf) (Wako Pure Chemical Industries), toluene (superdehydrated, Wako Pure Chemical Industries), tetrahydrofuran (THF) (superdehydrated, Wako Pure Chemical Industries), dichloromethane (superdehydrated, Wako Pure Chemical Industries), 2-propanol (Wako Pure Chemical Industries), anisole (Wako Pure Chemical Industries), *o*-dichlorobenzene (ODCB) (Wako Pure Chemical Industries), and heavily *n*-doped Si wafers (with a 300 nm-thick thermally grown SiO_2 layer, Electronics and Materials Corporation). Water was purified by Milli-Q ultrapure water system (Merck Direct-Q UV5).

3. OFET fabrication

Bottom-gate/top-contact type OFETs were fabricated using a *n*-doped silicon (Si) substrate with 300 nm thermally grown silicon dioxide (SiO_2; 11.3 nF/cm^2) as the gate dielectric. The substrates were ultrasonically washed with acetone, isopropanol, pure water and toluene for 5 min each. The washed substrates were subjected to UV–ozone treatment for 20 min. Then, 32 nm-thick parylene C was coated on the substrates. The total capacitance was estimated to be 10.4 nF/cm^2. **q2P** films were vacuum deposited on the substrate with the substrate temperature of at room temperature. The active layer thickness was 60 nm. Then, 45 nm-thick Au was vacuum deposited as the source/drain (S/D) electrode on the organic films through a metal mask. The S/D channel lengths (L) was 100 μm and the width (W) was 500 μm. **q2P^{Hex}** crystalline films were fabricated by blade-coating method. The coating conditions were as follows; 0.15 wt% anisole solution was deposited on a 27 nm-thick parylene C coated substrate (total capacitance: 10.6 nF/cm^2) at 80 °C and sheared by a glass blade with a speed of 6 cm/h, 0.15 wt% ODCB solution was deposited

on a 30 nm-thick parylene C coated substrate (total capacitance: 10.5 nF/cm^2) at 110 °C and sheared by a glass blade with a speed of 8 cm/h. 45 nm-thick Au was vacuum deposited as the S/D electrode on the organic films through a metal mask. The *L*/*W* was 100/500 μm for the film using 0.15 wt% anisole solution and was 50/67–500 μm for the film using 0.15 wt% ODCB solution. Thermal annealing was performed at 110 °C overnight under N_2 atmosphere. Spin-coated **q2P^{Hex}** films were fabricated under the following conditions; 0.20 wt% anisole solution was deposited on a 30 nm-thick parylene C coated substrate (total capacitance: 10.5 nF/cm^2) preheated to 80 °C and spun at 1,000 rpm for 180 s. Thermal annealing was performed at 110 °C overnight under N_2 atmosphere. 80 nm-thick Au was vacuum deposited as the S/D electrode on the organic films through a metal mask. The *L*/*W* was 50/500 μm.

4. Detailed synthetic procedures

5,5′-Dibromo-2,2′-bis[3,4-(2,2-dimethylpropylenedioxy)thiophene] (2a)

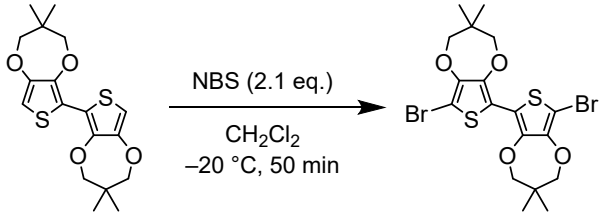

1a **2a**, 95%

To a solution of compound **1a**[S1] (366 mg, 1.00 mmol) in dichloromethane (35 mL) was added a solution of NBS (374 mg, 2.1 mmol) in dichloromethane (15 mL) slowly at −20 °C. The reaction mixture was stirred for 50 min at the temperature. After the addition of saturated aqueous sodium bicarbonate (40 mL), the mixture was allowed to warm to room temperature and extracted with dichloromethane (3 × 50 mL). After addition of aqueous solution of sodium thiosulfate (0.2 M, 170 mL) to the combined organic layer, the mixture was stirred vigorously for 30 min at room temperature. The mixture was extracted with dichloromethane (3 × 50 mL), dried over anhydrous sodium sulfate, and concentrated in vacuo. The residue was purified by silica gel column chromatography (eluent: dichloromethane/hexane = 1:1) to afford compound **2a** as a white to pale yellow solid (499 mg, 0.952 mmol, 95% yield). Physical properties of **2a**: ^{1}H NMR ($CDCl_3$, 400 MHz): δ 1.07 (s, 12H), 3.81 (s, 4H), 3.83 (s, 4H); ^{13}C NMR ($CDCl_3$, 100 MHz): δ 21.6, 39.1, 80.2, 80.5, 92.9, 114.9, 144.0, 147.3; HRMS (FD) calcd for $C_{18}H_{20}Br_2O_4S_2$ [M$^{\bullet+}$] 523.9144, found: 523.9124. The structural integrity and purity were identified by NMR spectra (Fig. S13 and S14).

2-[(5*E*)-3,4-(2,2-Dimethylpropylenedioxy)-5-[3,4-(2,2-dimethylpropylenedioxy)-5-(dicyanomethylene)-2(5*H*)-thienylidene]-2(5*H*)-thienylidene]propanedinitrile (q2P)

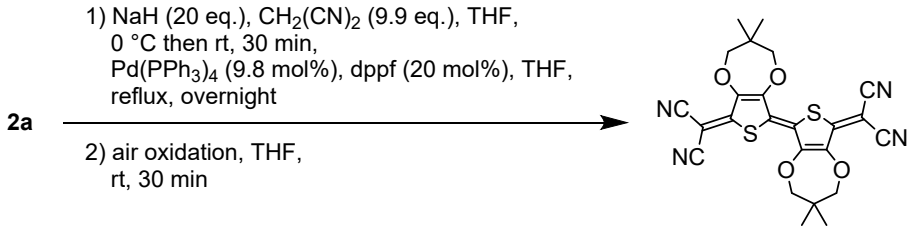

q2P, 24% (2 steps)

To the solution of malononitrile (130 mg, 1.97 mmol) in THF (25 mL) was added sodium hydride (60% dispersion in mineral oil, 158 mg, 3.95 mmol) at 0 °C. The reaction mixture was allowed to warm to room temperature and

stirred for 30 min. After the addition of $Pd(PPh_3)_4$ (22.6 mg, 19.6 μmol) and dppf (22.7 mg, 40.9 μmol) to the reaction mixture, a solution of compound **2a** (105 mg, 200 μmol) in THF (40 mL) was added dropwise for 20 min to the reaction mixture. The mixture was stirred at the reflux temperature overnight. Then, 2 M HCl aq. (3 mL) was added at 0 °C. After stirred for 30 min in air, the mixture was extracted with dichloromethane (3 × 100 mL). The collected extracts were combined and washed subsequently with water (3 × 70 mL) and brine (3 × 70 mL), dried over anhydrous sodium sulfate, and concentrated in vacuo. The residue was roughly purified by silica gel column chromatography (eluent: dichloromethane) and subsequently purified by GPC (eluent: chloroform) to afford **q2P** as a purple solid (24.0 mg, 48.7 μmol, 24% yield for two-step transformations). For the use for device application, **q2P** was finally purified by washing with ethyl acetate and methanol and recrystallizing several times with slow cooling from chlorobenzene solution, affording metallic purple needle-like single crystals. Physical properties of **q2P**: ^{1}H NMR ($CDCl_3$, 400 MHz): δ 1.12 (s, 12H), 4.02 (s, 4H), 4.10 (s, 4H); ^{13}C NMR assignment could not be characterized due to its poor solubility for solvents such as DMSO-d_6); HRMS (FD): calcd for $C_{24}H_{20}N_4O_4S_2$ [$M^{\bullet+}$] 492.0920, found: 492.0932. The structural integrity was identified by ^{1}H NMR spectra (Fig. S15) and single-crystal XRD structural analysis (Fig. 3 and S3 and Table S2), confirming *E* configuration.

5,5′-Dibromo-2,2′-bis[3,4-(2,2-dihexylpropylenedioxy)thiophene] (2b)

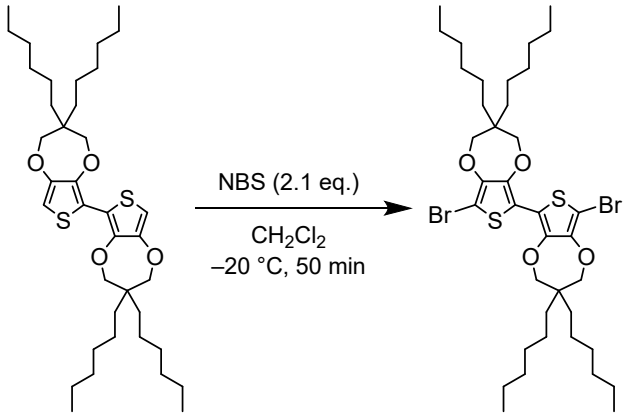

To the solution of compound **1b**[S2–S6] (453 mg, 0.700 mmol) in dichloromethane (25 mL) was added a solution of NBS (262 mg, 1.47 mmol) slowly at −20 °C. The reaction mixture was stirred for 50 min at the temperature. After the addition of saturated aqueous sodium bicarbonate (30 mL), the mixture was allowed to warm to room temperature and extracted with dichloromethane (3 × 50 mL). After addition of aqueous solution of sodium thiosulfate (0.2 M, 120 mL) to the combined organic layer, the mixture was stirred vigorously for 30 min at the temperature. The mixture was extracted with dichloromethane (3 × 50 mL), dried over anhydrous sodium sulfate, and concentrated in vacuo. The residue was purified by silica gel column chromatography (eluent: dichloromethane/hexane = 1:6) to afford compound **2b** as a pale yellow solid (479 mg, 0.595 mmol, 85% yield). Physical properties of **2b**: ^{1}H NMR ($CDCl_3$, 400 MHz): δ 0.89 (t, J = 6.8 Hz, 12H), 1.20–1.34 (m, 32H), 1.36–1.45 (m, 8H), 3.91 (s, 4H), 3.92 (s, 4H); ^{13}C NMR ($CDCl_3$, 100 MHz): δ 14.1, 22.7, 22.7, 30.1, 31.7, 43.9, 78.1, 78.2, 91.9, 114.3, 143.8, 147.2; HRMS (FD): calcd for $C_{38}H_{60}Br_2O_4S_2$ [$M^{\bullet+}$] 804.2277, found: 804.2296. The structural integrity and purity were identified by NMR spectra (Fig. S16 and S17).

2-[(5*E*)-3,4-(2,2-Dihexylpropylenedioxy)-5-[3,4-(2,2-dihexylpropylenedioxy)-5-(dicyanomethylene)-2(5*H*)-thienylidene]-2(5*H*)-thienylidene]propanedinitrile (q2P^{Hex})

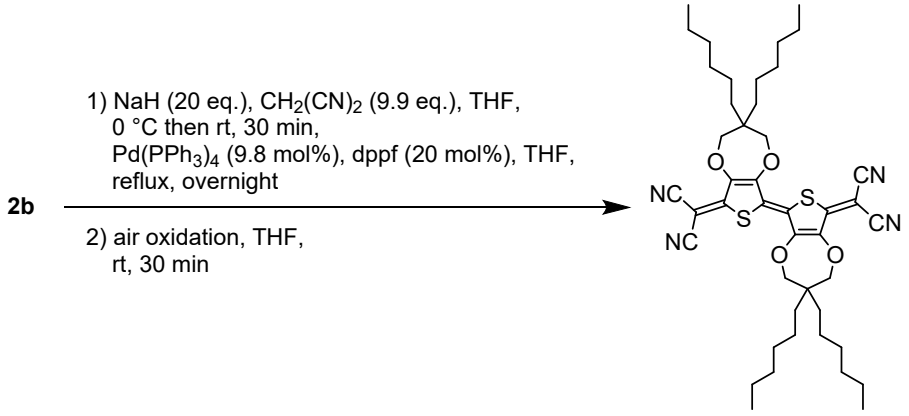

q2P^{Hex}, 12% (2 steps)

To the solution of malononitrile (325 mg, 4.93 mmol) in THF (63 mL) was added sodium hydride (60% dispersion in mineral oil, 395 mg, 9.88 mmol) at 0 °C. The reaction mixture was stirred for 30 min at room temperature. After the addition of $Pd(PPh_3)_4$ (56.6 mg, 49.0 μmol) and dppf (56.7 mg, 102 μmol) to the reaction mixture, a solution of compound **2b** (402 mg, 0.500 mmol) in THF (100 mL) was added dropwise for 20 min to the reaction mixture. The mixture was refluxed overnight. Then, 2 M HCl aq. (8 mL) was added at 0 °C. After stirred for 30 min in air, the mixture was extracted with dichloromethane (3 × 70 mL). The collected extracts were washed subsequently with water (3 × 70 mL) and brine (3 × 70 mL), dried over anhydrous sodium sulfate, and concentrated in vacuo. The residue was roughly purified by silica gel column chromatography (eluent: toluene) to afford purple crude material. The crude material was purified by GPC (eluent: chloroform) to afford **q2P^{Hex}** as a purple solid (46.0 mg, 59.0 μmol, 12% yield for two-step transformations). For the use for device application, **q2P^{Hex}** was finally purified by washing with a small amount of ethyl acetate and methanol and recrystallizing several times with dichloromethane/methanol liquid-liquid dispersion method, affording metallic purple single crystals. Physical properties of **q2P^{Hex}**: ^{1}H NMR ($CDCl_3$, 400 MHz): δ 0.90 (t, J = 6.8 Hz, 12H), 1.23–1.35 (m, 32H), 1.37–1.46 (m, 8H), 4.10 (s, 4H), 4.18 (s, 4H); ^{13}C NMR ($CDCl_3$, 100 MHz): δ 14.0, 22.6, 22.7, 29.9, 31.6, 31.9, 43.3, 68.1, 80.0, 80.7, 112.1, 113.5, 123.5, 159.7, 144.8, 150.4; HRMS (FD): calcd for $C_{44}H_{60}N_4O_4S_2$ [$M^{\bullet+}$] 772.4050, found: 772.4046. The structural integrity and purity were identified by ^{1}H and ^{13}C NMR spectra (Fig. S18 and S19). The structural integrity was further analyzed by the single-crystal XRD structural analysis (Fig. 3 and S3 and Table S2), which confirmed *E* configuration.

5. Electrochemical and optical properties

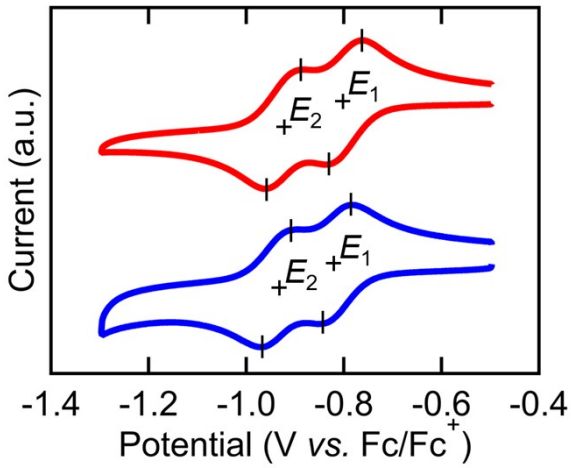

Fig. S1 Cyclic voltammograms of **q2P** (red line) and **q2P^{Hex}** (blue line). The first and the second reduction potentials (E_1 and E_2, respectively) were determined by half-wave potentials estimated by the average of the peak-top potentials.

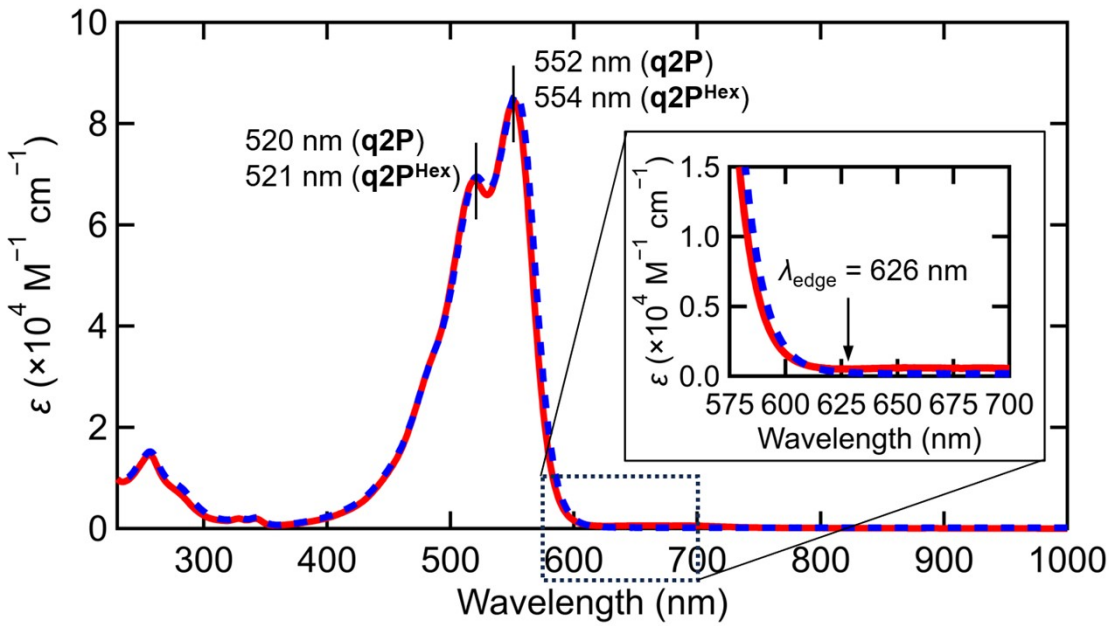

Fig. S2 UV–vis spectra of **q2P** (red line) and **q2P^{Hex}** (blue dashed line) in dichloromethane (**q2P**: 22.7 μM, **q2P^{Hex}** 21.3 μM).

6. DFT and TD-DFT calculations

The highest occupied molecular orbital (HOMO) and lowest unoccupied molecular orbitals (LUMO) of **q*n*P** (*n* = 2–5) and **q2P^{Hex}** were calculated based on density functional theory (DFT) at the RB3LYP/6-31G+(d) level using the Gaussian16 program,[S7] based on the optimized atomic coordinates (Tables S6–S10). With the geometries of **q2P** and **q2P^{Hex}**, time-dependent (TD)-DFT calculations were carried by using the RB3LYP/6-31G+(d) to estimate their absorption wavelength, oscillator strengths, and transition configurations in the transitions (Table S1).

Table S1 The absorption wavelengths (λ), oscillator strengths (f), and transition configurations of **q2P** and **q2P^{Hex}** calculated by TD-DFT method (RB3LYP/6-31G+(d)).

Compound	λ (nm)	f	Transition configuration (CI coefficient)
q2P	519.51	1.2887	HOMO → LUMO (0.72164)
	271.85	0.1414	HOMO−4 → LUMO (0.11405)
			HOMO−1 → LUMO+1 (0.65239)
			HOMO → LUMO+2 (−0.15938)
			HOMO → LUMO+4 (0.14025)
	241.70	0.1252	HOMO−13 → LUMO (0.24750)
			HOMO−12 → LUMO (0.20307)
			HOMO−10 → LUMO (−0.21904)
			HOMO−8 → LUMO (−0.16897)
			HOMO−6 → LUMO (−0.14512)
			HOMO−4 → LUMO (0.15024)
			HOMO−3 → LUMO+1 (0.35852)
			HOMO → LUMO+2 (0.22529)
			HOMO → LUMO+4 (−0.14631)
			HOMO → LUMO+5 (−0.16855)
q2P^{Hex}	526.09	1.1514	HOMO → LUMO (0.71671)
	280.03	0.0868	HOMO−16 → LUMO (−0.12878)
			HOMO−8 → LUMO (−0.37546)
			HOMO−1 → LUMO+1 (0.49105)
			HOMO → LUMO+3 (−0.22438)
			HOMO → LUMO+4 (0.12526)
	276.02	0.0856	HOMO−14 → LUMO (−0.11641)
			HOMO−9 → LUMO (0.13121)
			HOMO−8 → LUMO (0.45586)
			HOMO−1 → LUMO+1 (0.41012)
			HOMO → LUMO+4 (−0.21497)

7. Crystal structures and molecular coordinates

Table S2 Crystallographic data of **q2P** and **q2P^{Hex}**.

Compound	**q2P**	**q2P^{Hex}**
Chemical formula	$C_{24}H_{20}N_4O_4S_2$	$C_{44}H_{60}N_4O_4S_2$
Formula weight	492.56	773.08
Shape	Needle	Needle
Crystal system	Monoclinic	Triclinic
Space group	$P2_1/c$	$P-1$
a (Å)	10.1260(10)	5.7516(5)
b (Å)	6.4978(6)	11.9089(9)
c (Å)	17.491(2)	17.9175(15)
α (°)	90	105.893(7)
β (°)	98.052(11)	97.758(7)
γ (°)	90	102.381(7)
Volume (Å^3)	1139.5(2)	1128.12(17)
Z	2	1
D_{calc} (g/cm^3)	1.436	1.138
R_1 ($I > 2\sigma(I)$)	0.0694	0.0576
wR_2 (all reflections)	0.1896	0.1560
Reflections ($I > 2\sigma(I)$)	1295	3025
Temperature (K)	300	300
CCDC number	2413270	2413271

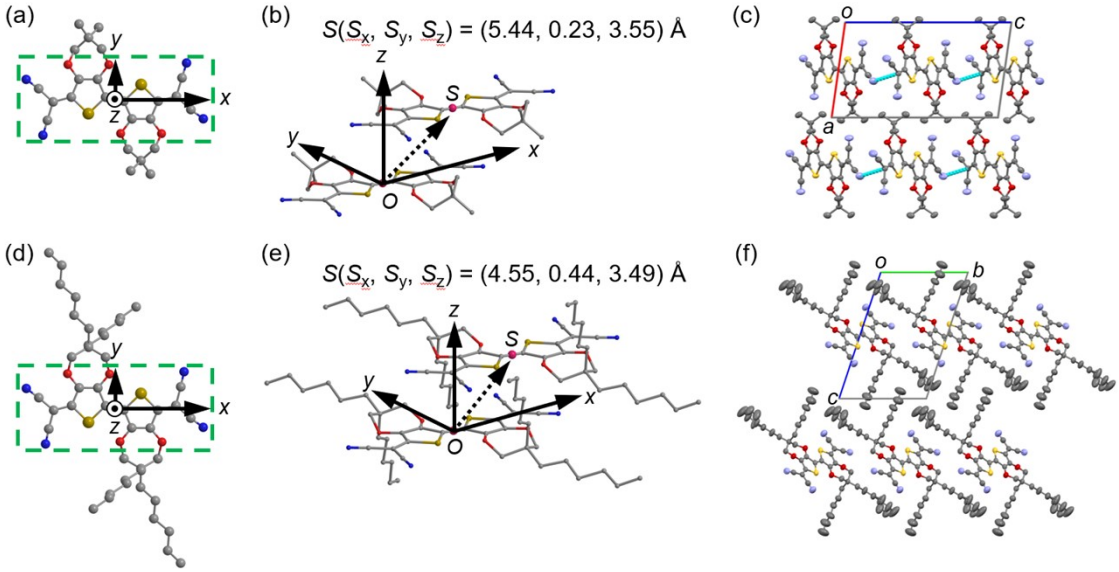

Fig. S3 (a, b, d, and e) Molecular coordinates and (c and f) crystal structures of **q2P** and **q2P^{Hex}**. The *x*- and *y*-axis correspond to the long- and short-molecular axis direction of the π-conjugated core, respectively. The *xy*-plane corresponds to the π-conjugated plane of 24 atoms involved in two thiophene rings, two dicyanomethylene substituents, and four oxygen atoms. The purple spheres represent the center of mass the molecules. At the point *S*, S_x and S_y represent the molecular slipping distances along the long- and short-molecular axis, respectively. S_z corresponds to π–π distance. Yellow: S, red: O, grey: C, pale blue: N. Hydrogen atoms are omitted for clarity. The pale blue dotted lines represent intermolecular C···N contacts. (a, b, d, and e) Ball and stick drawings and (c and f) ORTEP drawings (50% thermal ellipsoid) were shown.

8. Hirshfeld surface analyses

The Hirshfeld surface analysis was performed using the Crystal Explorer program[S8] based on the single-crystal structures of **q2P** and **q2P^{Hex}**. The d_e mapping revealed the densely packed via the intermolecular C···N contact and the intermolecular invasions of dialkylpropylenedioxy substituents to the molecular voids (Fig. S4).

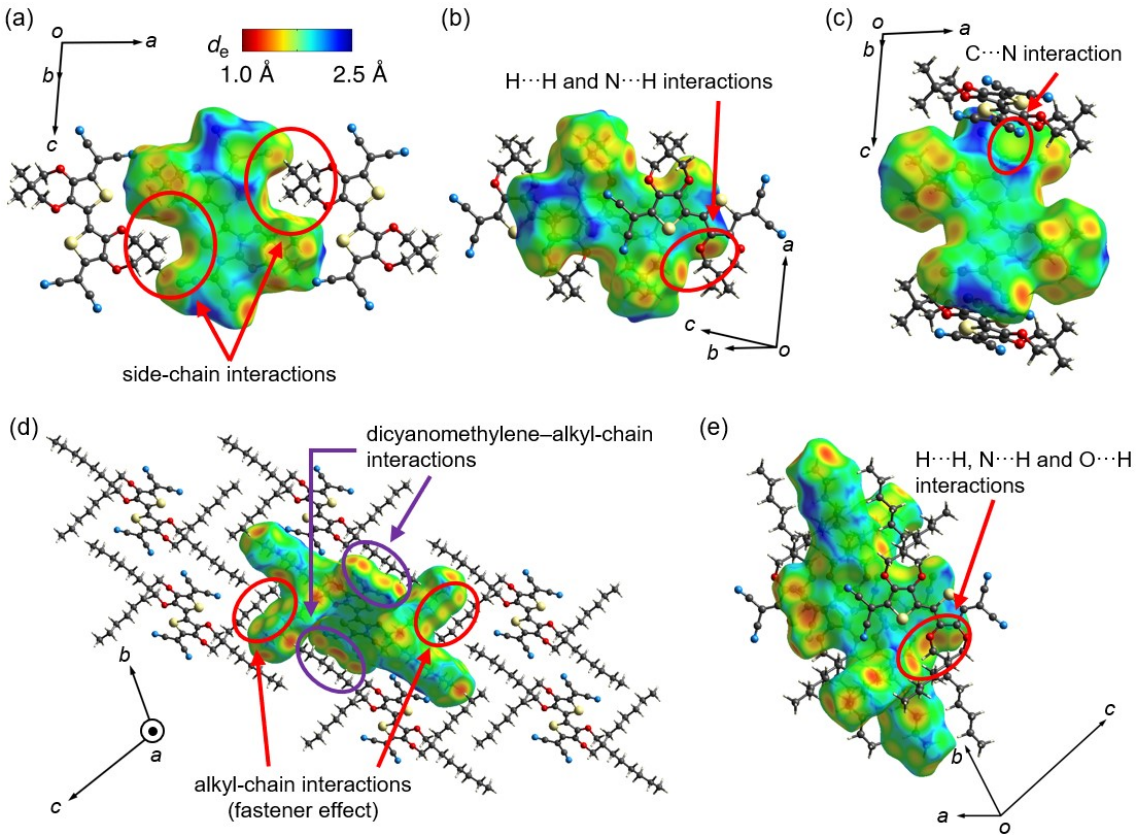

Fig. S4 Hirshfeld surface analyses (d_e mapping) of (a, b, and c) **q2P** and (d and e) **q2P^{Hex}**. Here, d_e indicates the distance from the Hirshfeld surface to the nearest nucleus outside the surface.

9. Thin-film properties

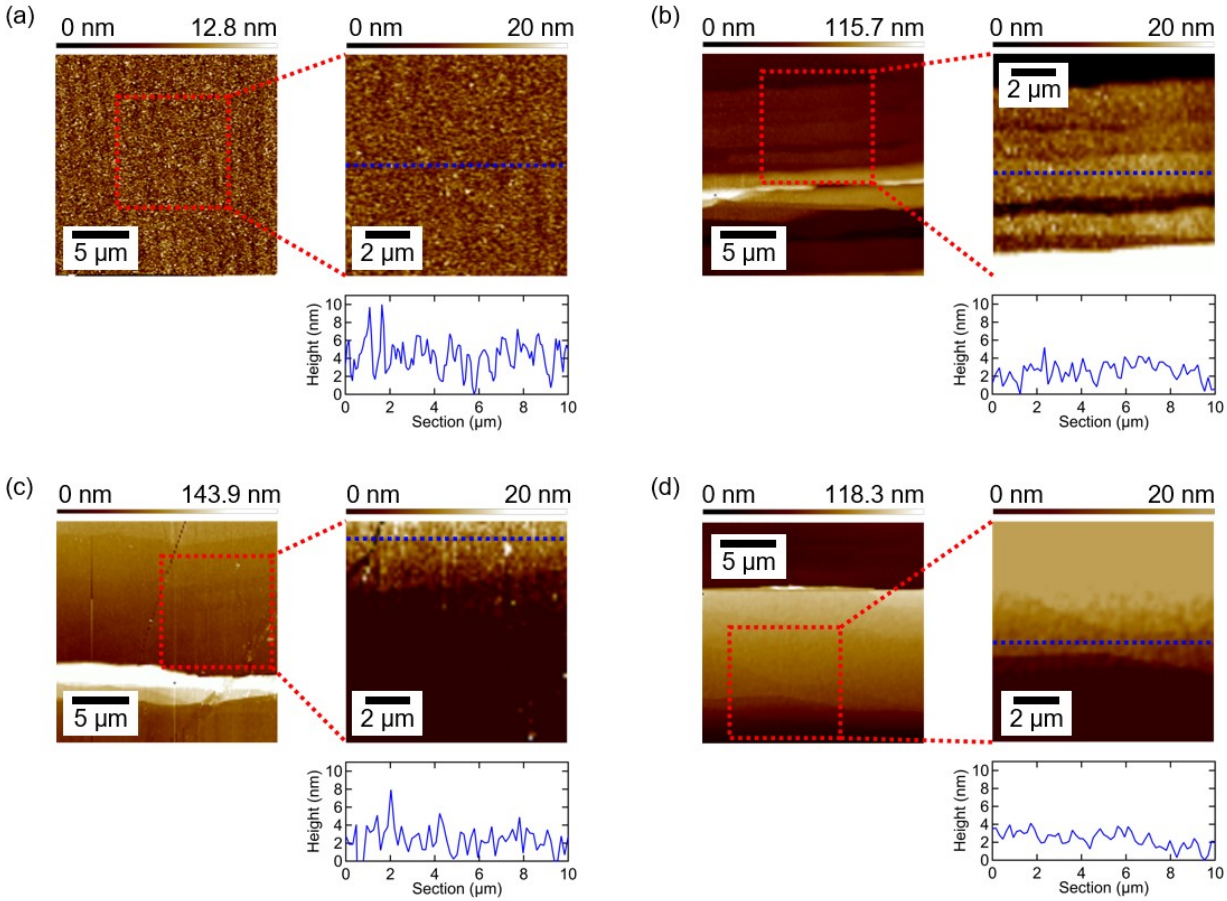

Fig. S5 AFM images of (a) a vacuum-deposited **q2P** film (root mean-square roughness (R_{rms}): 1.65 nm), (b) a blade-coated **q2P^{Hex}** film from 0.15 wt% anisole solution (R_{rms}: 1.07 nm), (c) a blade-coated **q2P^{Hex}** film from 0.15 wt% ODCB solution (R_{rms}: 1.04 nm), and (d) a blade-coated **q2P^{Hex}** film from 0.15 wt% ODCB solution (annealed, R_{rms}: 0.92 nm).

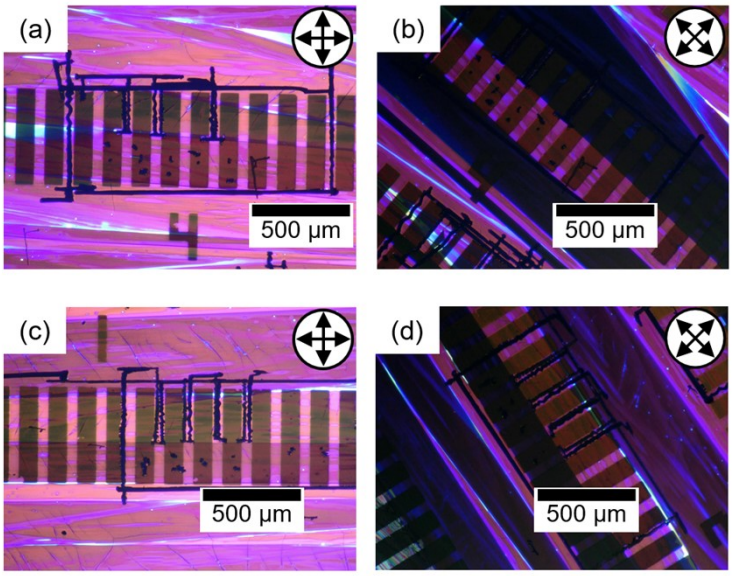

Fig. S6 Crossed Nicols polarized micrographs of a blade-coated **q2P^{Hex}** film from 0.15 wt% ODCB solution in (a) bright and (b) dark image and a blade-coated **q2P^{Hex}** film from 0.15 wt% ODCB solution (annealed) in (c) bright and (d) dark image.

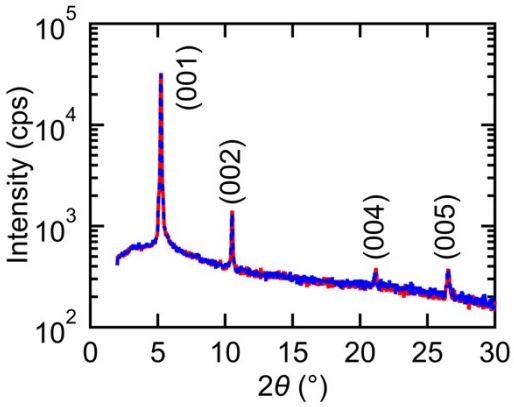

Fig. S7 PXRD patterns of **q2P^{Hex}** (a blade-coated film from 0.15 wt% ODCB solution). The blue dashed line and red line represent patterns before and after annealing, respectively.

10. OFET properties

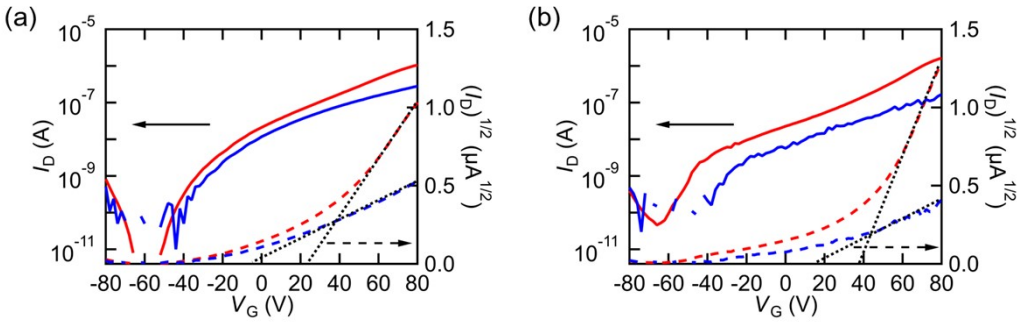

Fig. S8 Transfer characteristics (n-type) of (a) **q2P^{Hex}** (blade-coated film from 0.15 wt% ODCB solution) and (b) **q2P^{Hex}** (blade-coated film from 0.15 wt% ODCB solution, annealed). V_D = 80 V. The red and blue lines represent transfer characteristics in N_2 and air, respectively. The tangent lines for the V_G–$(I_D)^{1/2}$ curves were shown in black dashed lines.

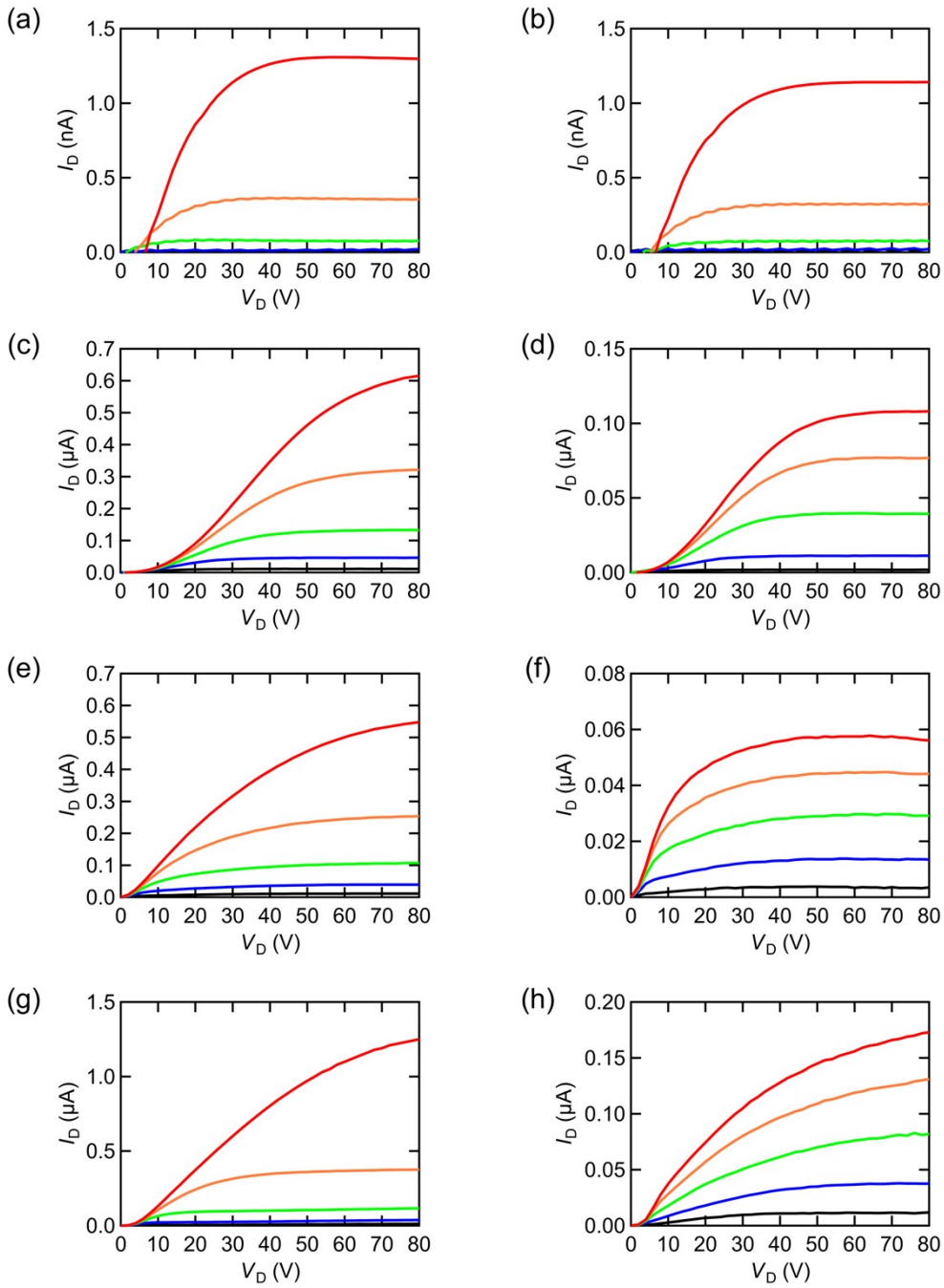

Fig. S9 Output characteristics (n-type) of (a) **q2P** (vacuum-deposited film, in vacuum), (b) **q2P** (vacuum-deposited film, in air), (c) **q2P^{Hex}** (blade-coated film from 0.15 wt% anisole solution, in vacuum), (d) **q2P^{Hex}** (blade-coated film from 0.15 wt% anisole solution, in air), (e) **q2P^{Hex}** (blade-coated film from 0.15 wt% ODCB solution, in N_2), (f) **q2P^{Hex}** (blade-coated film from 0.15 wt% ODCB solution, in air), (g) **q2P^{Hex}** (blade-coated film from 0.15 wt% ODCB solution, annealed, in N_2), and (h) **q2P^{Hex}** (blade-coated film from 0.15 wt% ODCB solution, annealed, in air). The black, blue, green, orange, and red lines represent output curves of V_G = 0, 20, 40, 60, and 80 V, respectively.

Table S3 OFET properties (n-type) of **q2P** and **q2P^{Hex}**.

Compound	Solvent	Condition	μ_{max} (cm^2/Vs)	μ_{avg} (cm^2/Vs)	V_{th} (V)	On/off ratio
q2P	—	Vac.	3.6×10^{-5}	3.5×10^{-5}	42	1.6×10^{2}
	—	Air	3.4×10^{-5}	3.2×10^{-5}	42	1.3×10^{2}
q2P^{Hex}	Anisole	Vac.	2.6×10^{-2}	1.6×10^{-2}	22	9.1×10^{4}
	Anisole	Air	1.9×10^{-2}	7.5×10^{-3}	14	1.1×10^{5}
	ODCB	N_2	1.5×10^{-2}	4.0×10^{-3}	4.5	1.1×10^{5}
	ODCB	Air	2.5×10^{-3}	8.1×10^{-4}	−11	7.6×10^{3}
	ODCB	N_2, annealed	4.6×10^{-2}	1.4×10^{-2}	22	4.5×10^{5}
	ODCB	Air, annealed	8.0×10^{-3}	2.5×10^{-3}	12	2.4×10^{4}

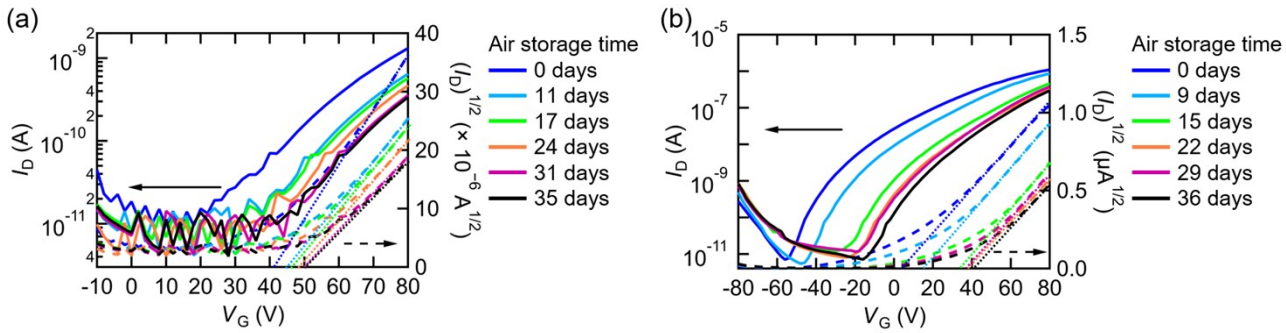

Fig. S10 Transfer characteristics (n-type) of (a) **q2P** (vacuum-deposited film) and (b) **q2P^{Hex}** (blade-coated film from 0.15 wt% anisole solution) over air storage time. Measurements were performed in air. V_D = 80 V. The tangent lines for the V_G–$(I_D)^{1/2}$ curves were shown in dashed lines.

Table S4 OFET properties (n-type) of **q2P** (vacuum-deposited film) and **q2P^{Hex}** (blade-coated film from 0.15 wt% anisole solution) over air storage time.

Compound	Air storage time (days)	μ_{max} (cm^2/Vs)	μ_{avg} (cm^2/Vs)	V_{th} (V)	On/off ratio
q2P	0	3.4×10^{-5}	3.2×10^{-5}	42	1.3×10^{2}
	11	2.1×10^{-5}	2.0×10^{-5}	46	1.4×10^{2}
	17	2.0×10^{-5}	1.9×10^{-5}	47	1.1×10^{2}
	24	1.9×10^{-5}	1.8×10^{-5}	48	1.1×10^{2}
	31	1.6×10^{-5}	1.5×10^{-5}	50	88
	35	1.6×10^{-5}	1.5×10^{-5}	49	95
q2P^{Hex}	0	1.9×10^{-2}	7.5×10^{-3}	14	1.1×10^{5}
	9	1.6×10^{-2}	9.3×10^{-3}	21	1.2×10^{5}
	15	1.2×10^{-2}	8.5×10^{-3}	28	9.8×10^{4}
	22	1.0×10^{-2}	7.1×10^{-3}	34	6.6×10^{4}
	29	1.3×10^{-2}	7.1×10^{-3}	32	5.5×10^{4}
	36	9.9×10^{-3}	6.4×10^{-3}	36	5.0×10^{4}

11. Thin-film and OFET properties of spin-coated q2P^{Hex} films

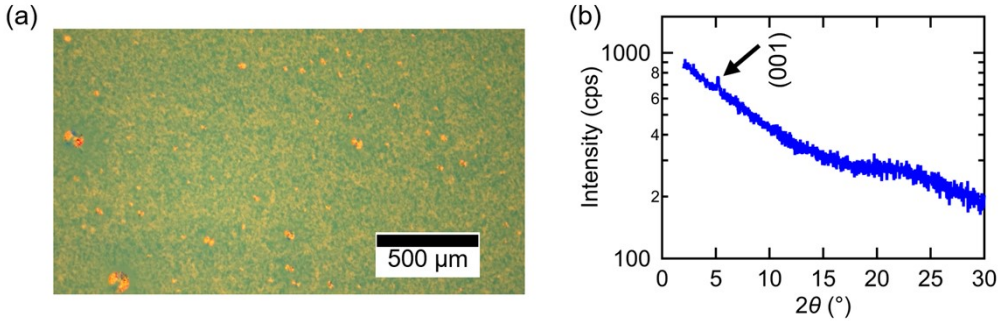

Fig. S11 (a) An optical image and (b) a PXRD pattern of a spin-coated **q2P^{Hex}** film.

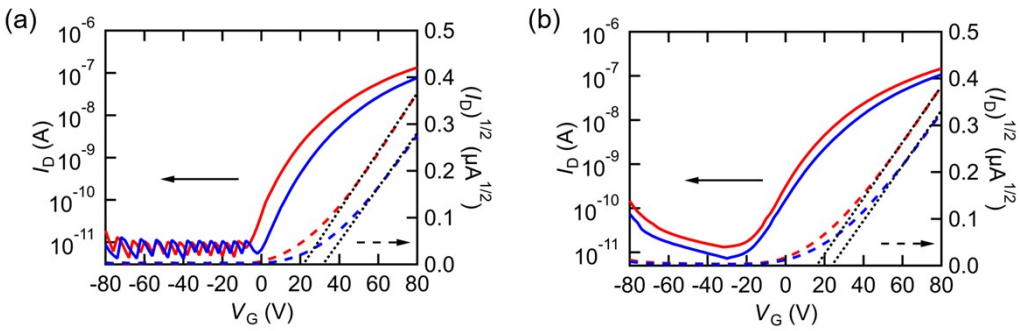

Fig. S12 Transfer characteristics (n-type) of spin-coated **q2P^{Hex}** (a) without annealing and (b) with annealing. V_D = 80 V. The red and blue lines represent transfer characteristics in vacuum and air, respectively. The tangent lines for the V_G–$(I_D)^{1/2}$ curves were shown in black dashed lines.

Table S5 OFET properties (n-type) of spin-coated **q2P^{Hex}**.

Condition	μ_{max} (cm^2/Vs)	μ_{avg} (cm^2/Vs)	V_{th} (V)	On/off ratio
Vac.	8.3×10^{-4}	7.5×10^{-4}	21	3.1×10^{4}
Air	6.7×10^{-4}	5.9×10^{-4}	33	1.7×10^{4}
Vac, annealed	1.1×10^{-3}	7.3×10^{-4}	17	1.4×10^{4}
Air, annealed	1.0×10^{-3}	6.6×10^{-4}	24	1.1×10^{4}

12. NMR spectra

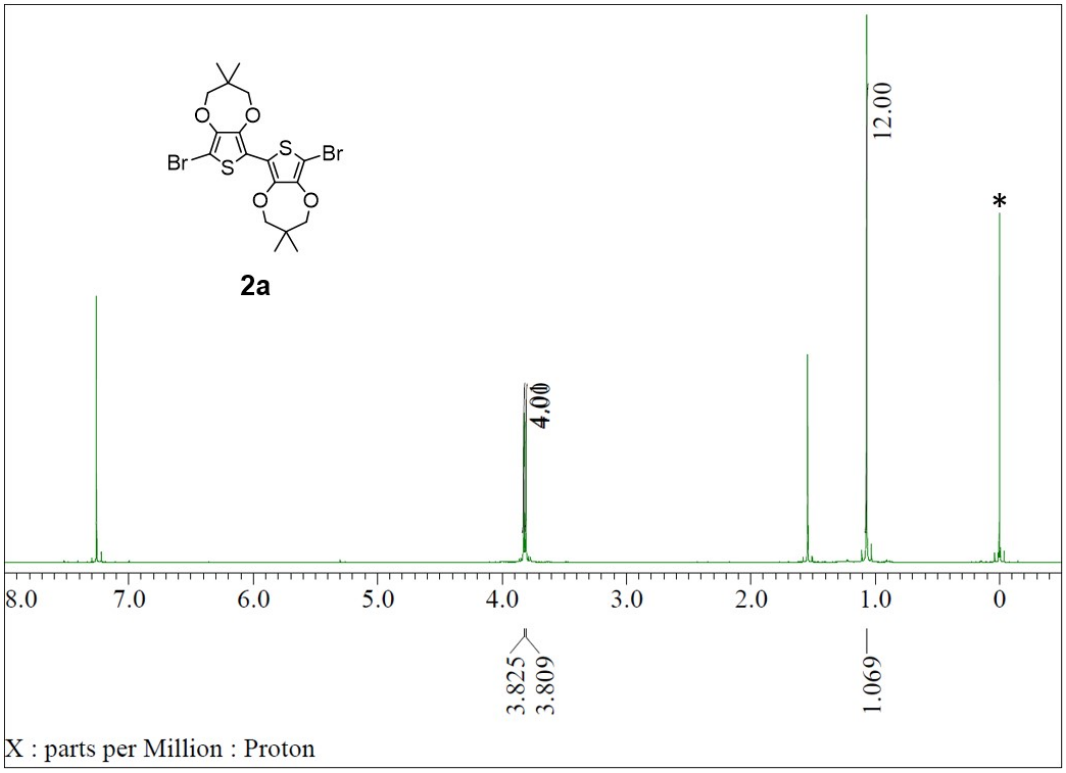

Fig. S13 ^{1}H NMR spectrum of compound **2a**. The signal for $Si(CH_3)_4$ used for the internal standard was shown with an asterisk.

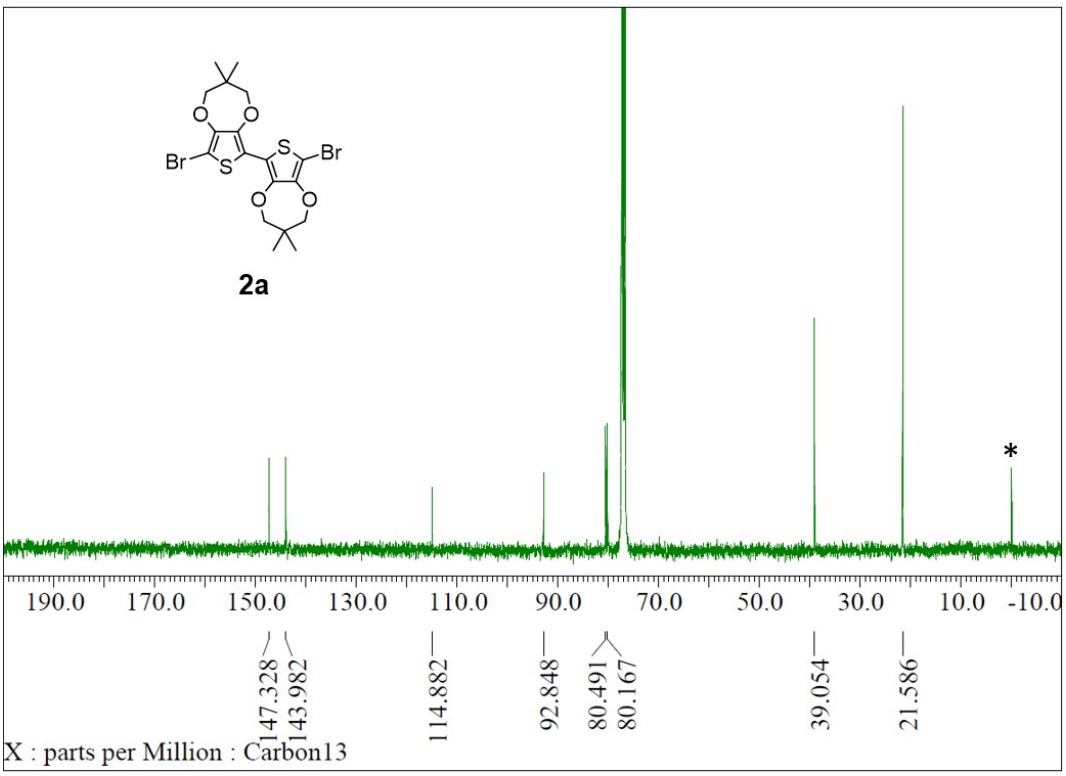

Fig. S14 ^{13}C NMR spectrum of compound **2a**. The signal for $Si(CH_3)_4$ used for the internal standard was shown with

an asterisk.

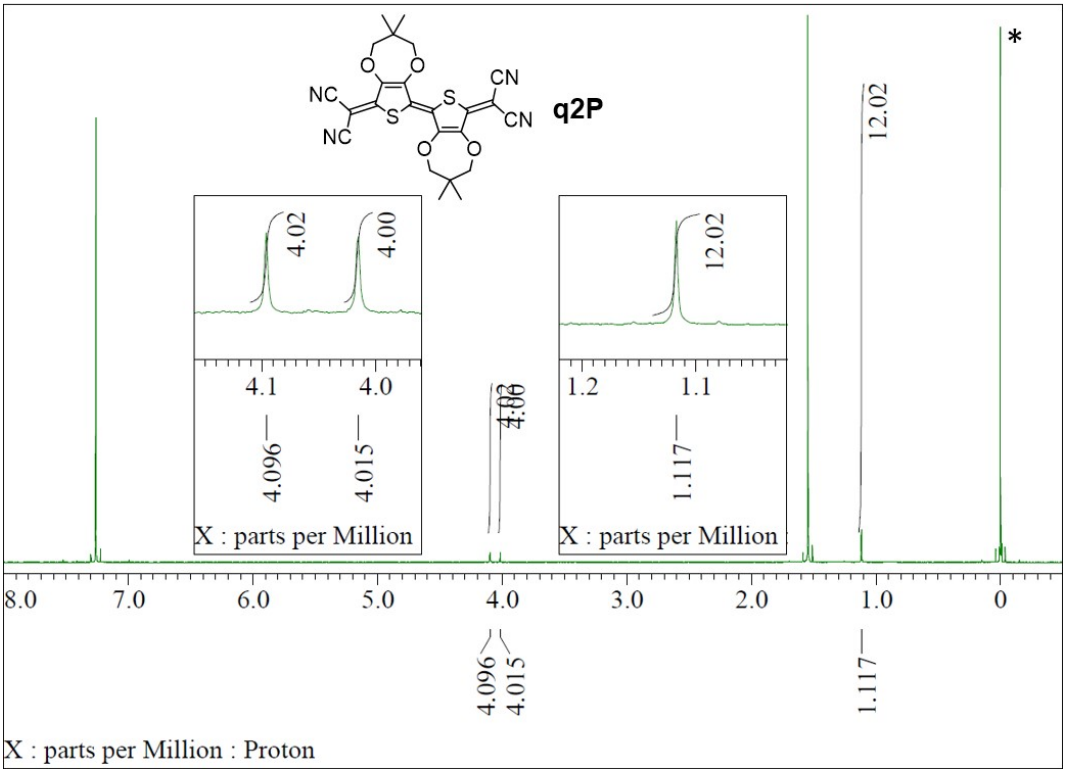

Fig. S15 ^{1}H NMR spectrum of **q2P**. The signal for $Si(CH_3)_4$ used for the internal standard was shown with an asterisk.

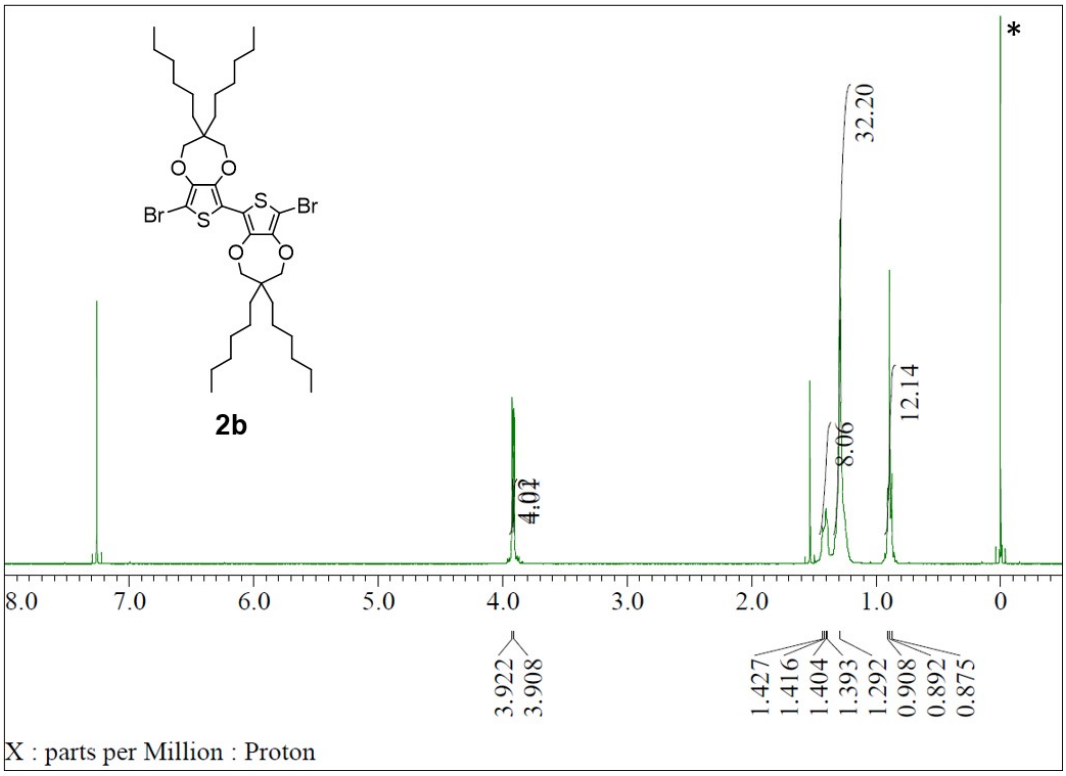

Fig. S16 ^{1}H NMR spectrum of compound **2b**. The signal for $Si(CH_3)_4$ used for the internal standard was shown with an asterisk.

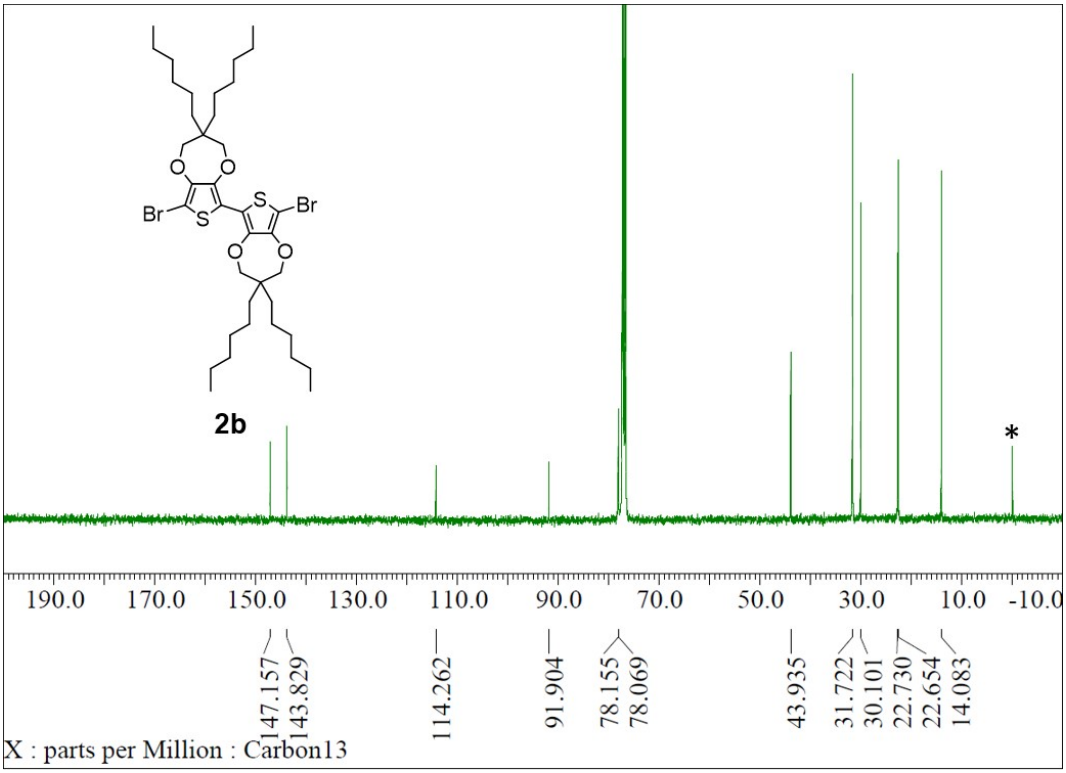

Fig. S17 ^{13}C NMR spectrum of compound **2b**. The signal for $Si(CH_3)_4$ used for the internal standard was shown with an asterisk.

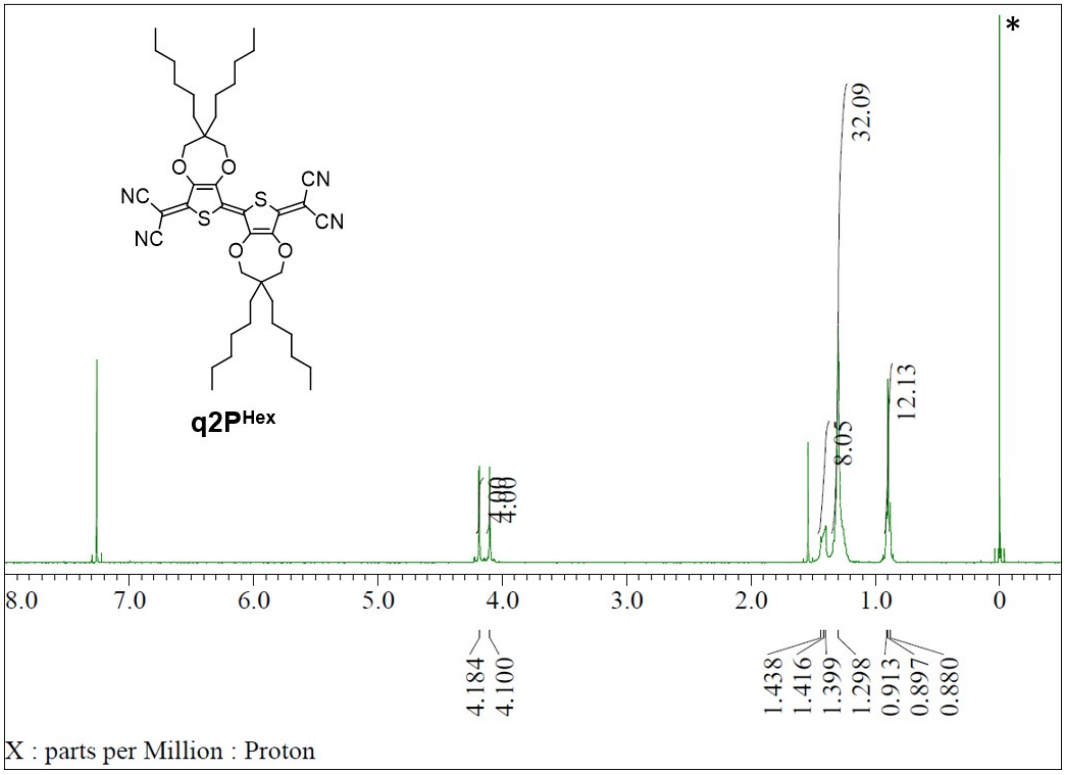

Fig. S18 ^{1}H NMR spectrum of **q2P^{Hex}**. The signal for $Si(CH_3)_4$ used for the internal standard was shown with an asterisk.

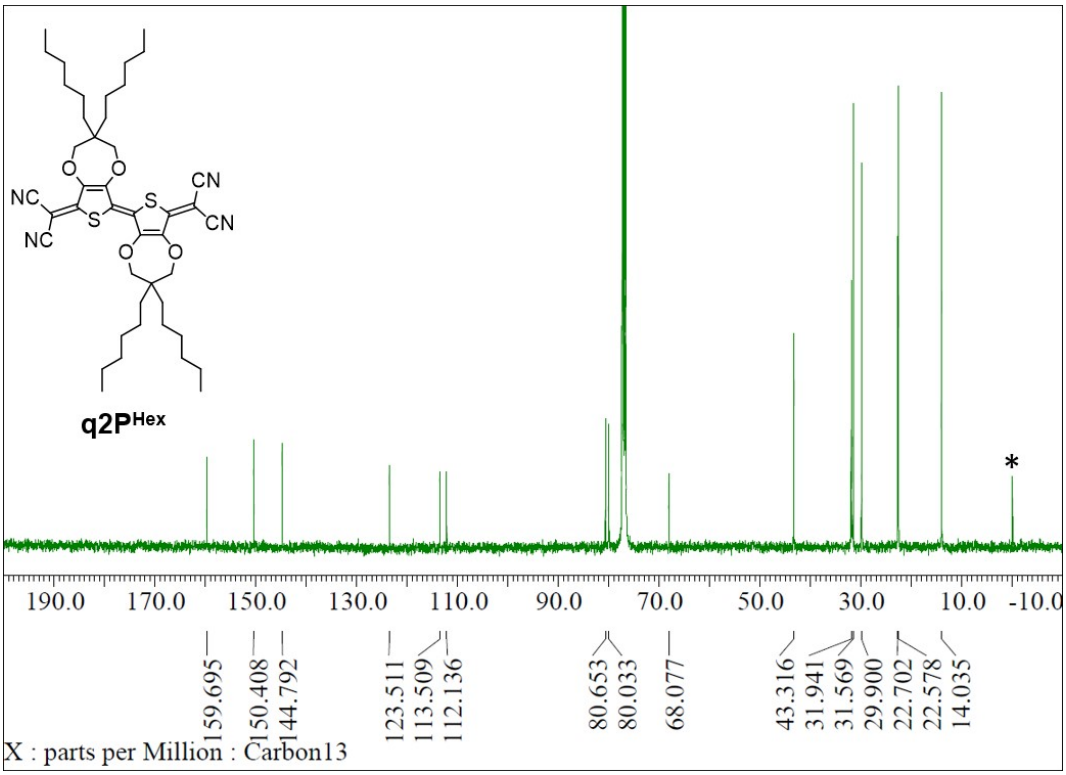

Fig. S19 ^{13}C NMR spectrum of **q2P^{Hex}**. The signal for $Si(CH_3)_4$ used for the internal standard was shown with an asterisk.

13. HRMS spectra

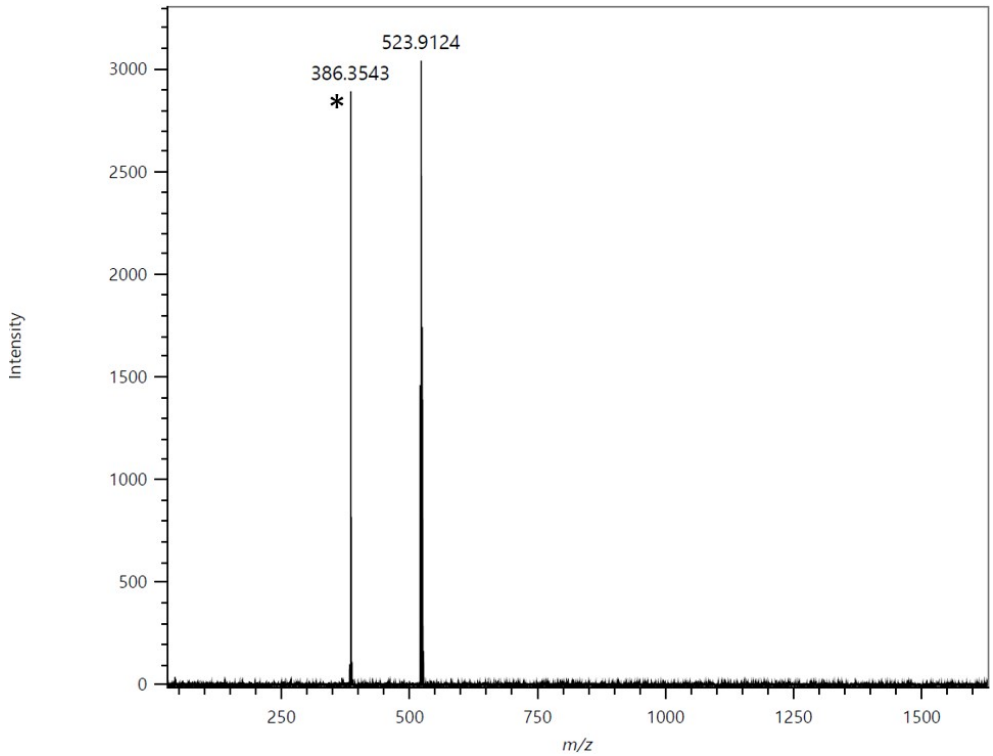

Fig. S20 HRMS spectrum of compound **2a**. The signal for cholesterol used for the internal standard was shown with an asterisk.

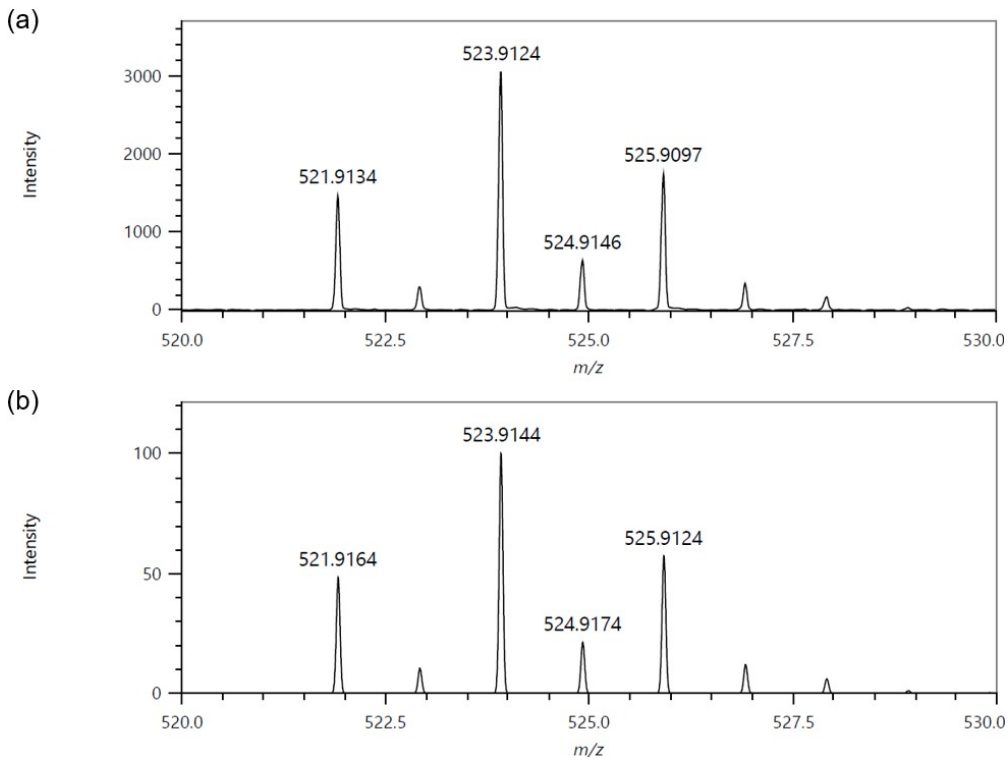

Fig. S21 Expanded HRMS spectra of compound **2a**. (a) An experimental spectrum. (b) A simulated spectrum.

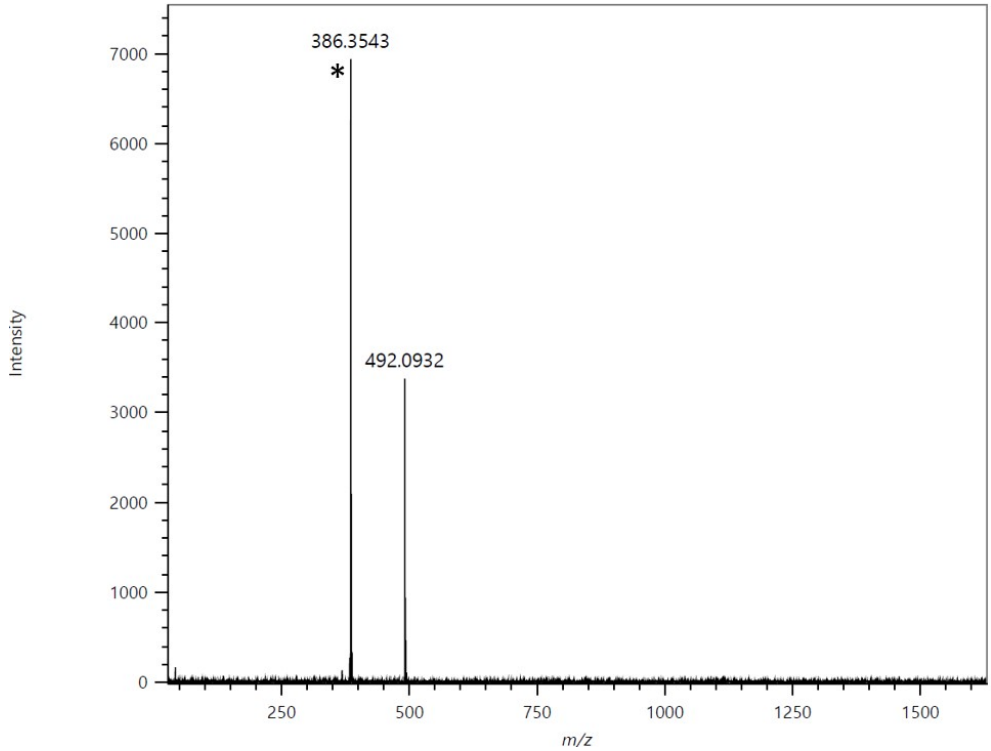

Fig. S22 HRMS spectrum of **q2P**. The signal for cholesterol used for the internal standard was shown with an asterisk.

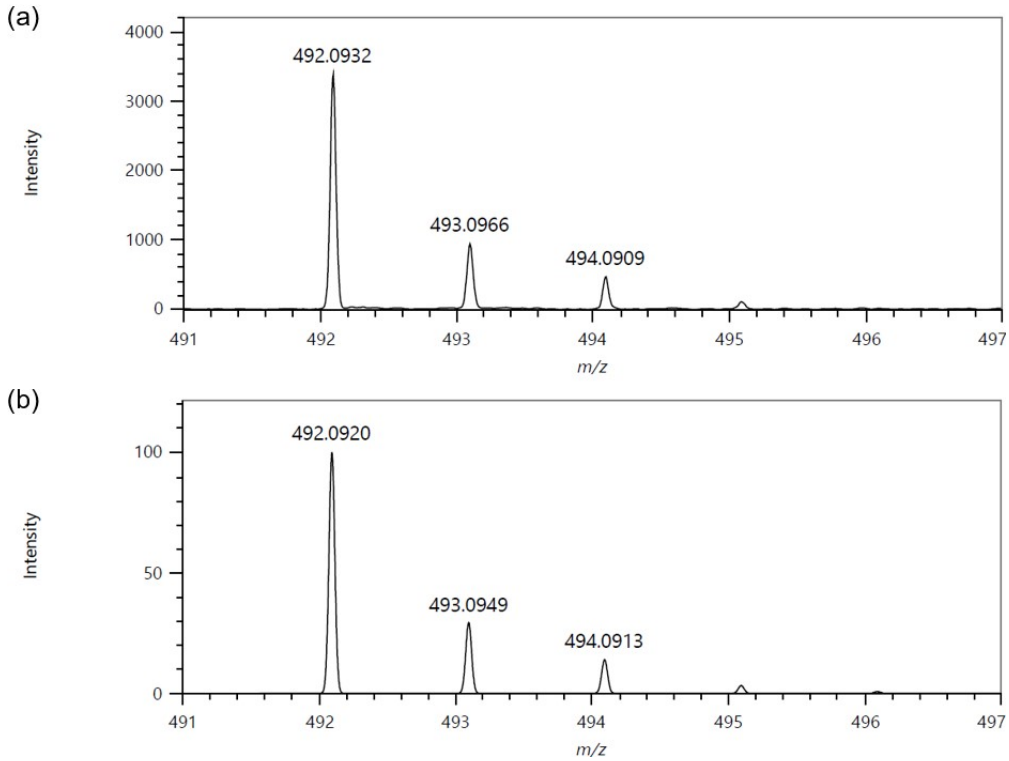

Fig. S23 Expanded HRMS spectra of **q2P**. (a) An experimental spectrum. (b) A simulated spectrum.

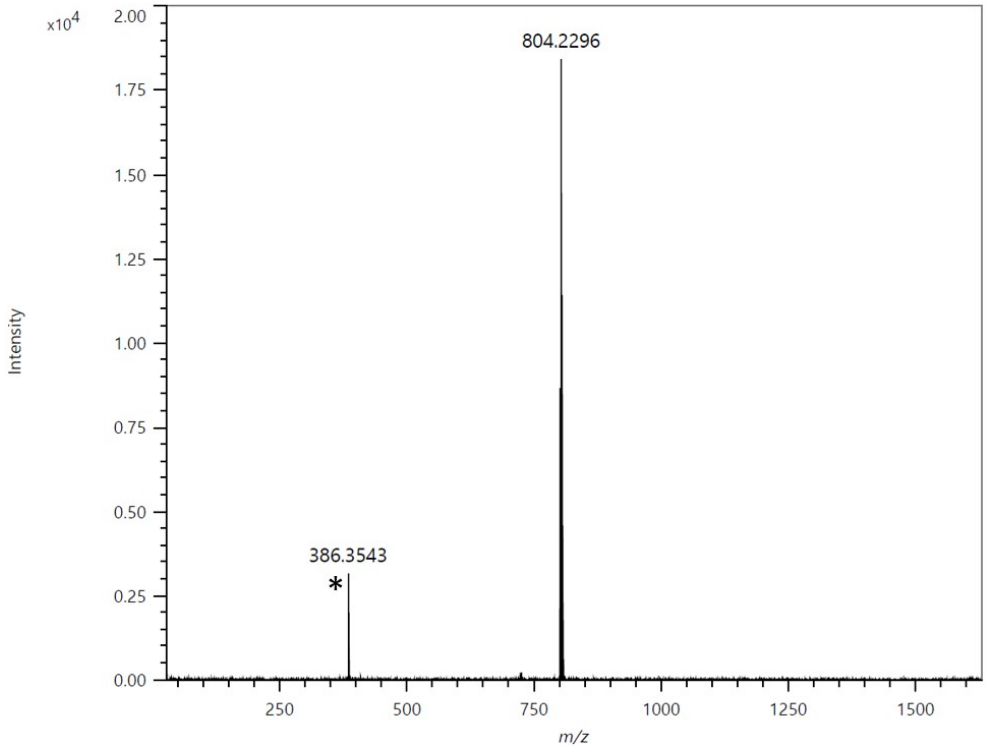

Fig. S24 HRMS spectrum of compound **2b**. The signal for cholesterol used for the internal standard was shown with an asterisk.

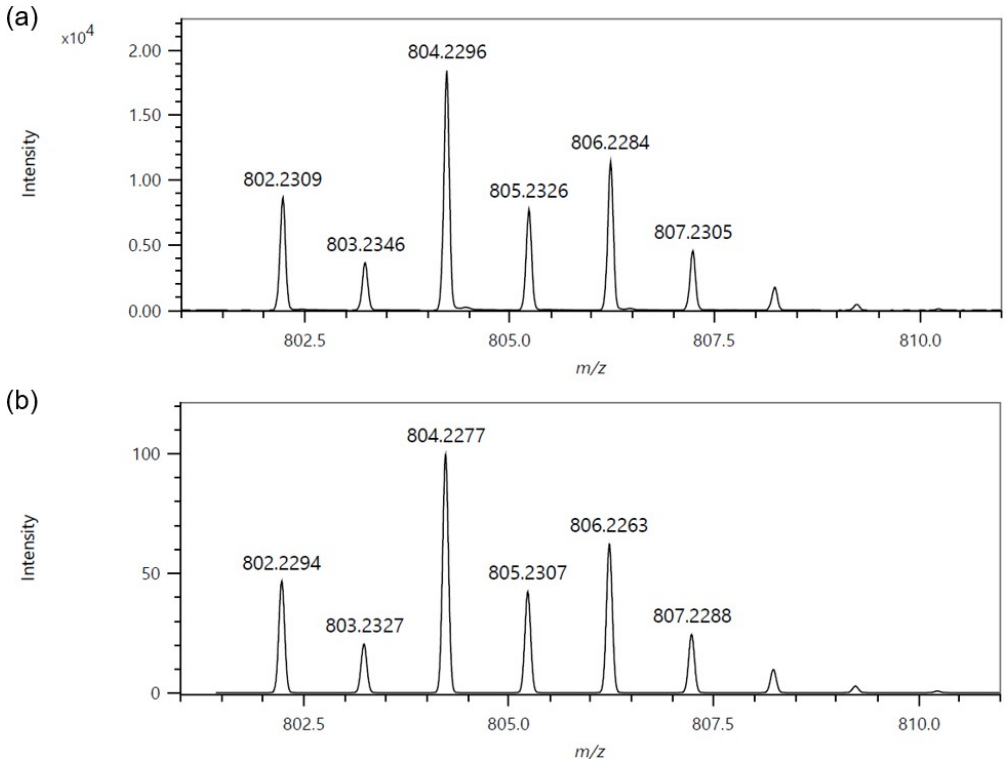

Fig. S25 Expanded HRMS compound **2b**. (a) An experimental spectrum. (b) A simulated spectrum.

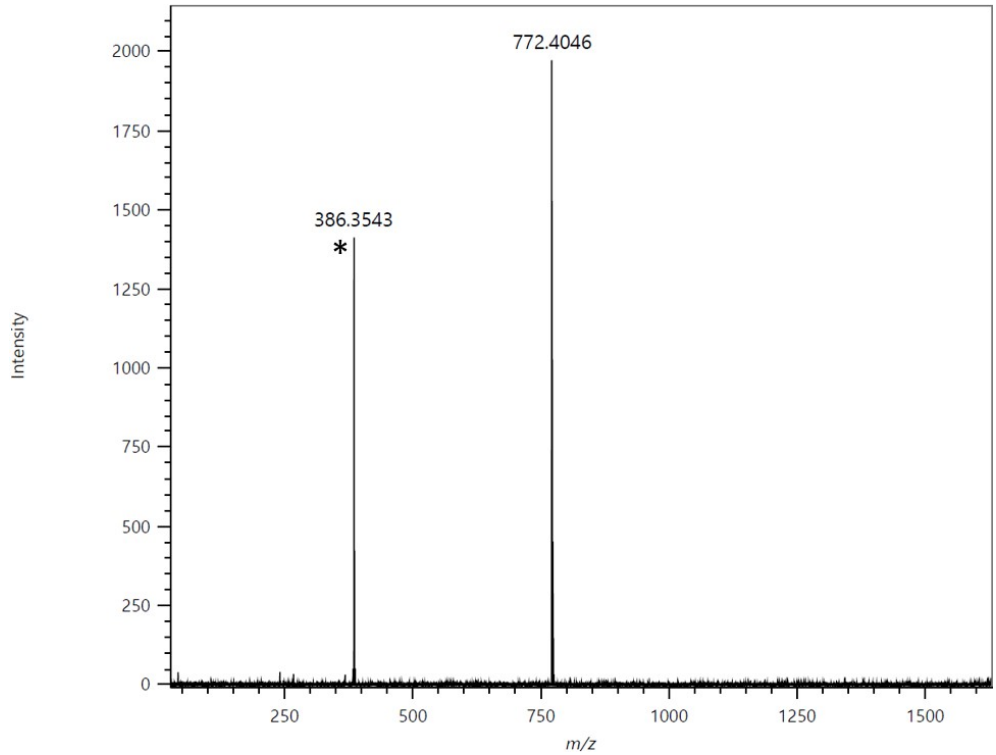

Fig. S26 HRMS spectrum of **q2P^{Hex}**. The signal for cholesterol used for the internal standard was shown with an asterisk.

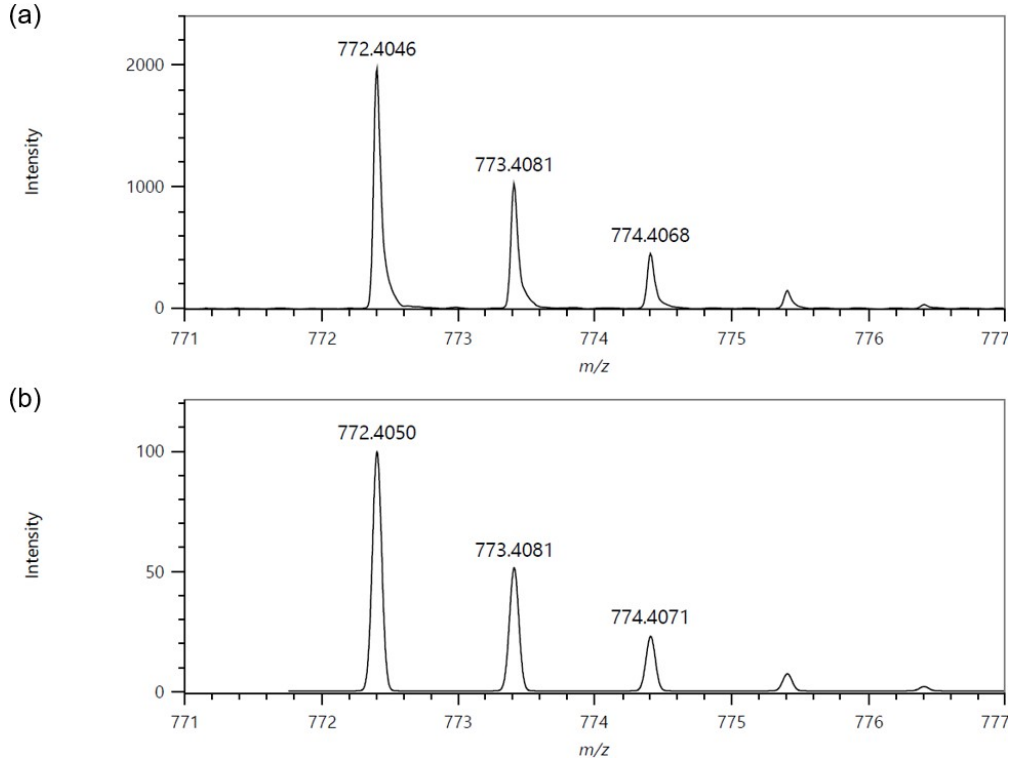

Fig. S27 Expanded HRMS spectra of **q2P^{Hex}**. (a) An experimental spectrum. (b) A simulated spectrum.

14. DFT calculation data

Table S6 Optimized atom coordination of **q2P** based on a DFT calculation (RB3LYP/6-31G+(d)).

Tag	Symbol	X	Y	Z
1	C	−2.02764	1.278355	1.828376
2	C	−2.82619	0.12447	1.506062
3	S	−1.96725	−0.96076	0.412145
4	C	−0.56322	0.130866	0.359451
5	C	−0.80223	1.280119	1.19672
6	O	−2.47647	2.150732	2.754438
7	O	0.19479	2.178154	1.35053
8	C	−2.34702	3.566153	2.517441
9	C	−0.1109	3.593067	1.342216
10	C	−0.90554	4.100679	2.556028
11	C	−0.99231	5.636517	2.417189
12	C	−0.2072	3.726386	3.875196
13	C	−4.10262	−0.16891	1.956756
14	C	−4.73013	−1.388	1.559738
15	C	−4.8707	0.693753	2.795718
16	N	−5.21448	−2.39222	1.218853
17	N	−5.56251	1.351979	3.46363
18	C	0.813535	−1.27371	−1.20535
19	C	0.574518	−0.12446	−0.36808
20	S	1.978539	0.967174	−0.42076
21	C	2.837499	−0.11806	−1.51466
22	C	2.038961	−1.27194	−1.83699
23	O	−0.18348	−2.17174	−1.35917
24	O	2.487802	−2.14431	−2.76305
25	C	0.122212	−3.58666	−1.35086
26	C	2.358346	−3.55973	−2.52606
27	C	0.91687	−4.09426	−2.56466
28	C	1.00364	−5.6301	−2.42583
29	C	0.218551	−3.71997	−3.88384
30	C	4.113941	0.175326	−1.96533
31	C	4.882034	−0.68734	−2.80428
32	N	5.57386	−1.34557	−3.47218
33	C	4.741442	1.394416	−1.5683
34	N	5.225787	2.398633	−1.22741
35	H	−2.94196	4.012591	3.317393

36	H	−2.82159	3.801327	1.554163
37	H	0.875101	4.062151	1.308864
38	H	−0.64224	3.820176	0.407691
39	H	0.007802	6.084458	2.431299
40	H	−1.55973	6.066697	3.250092
41	H	−1.4842	5.938416	1.48388
42	H	−0.13113	2.643439	4.004641
43	H	0.806641	4.142786	3.905103
44	H	−0.76349	4.128707	4.729802
45	H	−0.86378	−4.05574	−1.31752
46	H	0.653543	−3.81377	−0.41633
47	H	2.953304	−4.00617	−3.326
48	H	2.832913	−3.79491	−1.56277
49	H	1.571075	−6.06028	−3.25873
50	H	0.003532	−6.07804	−2.43995
51	H	1.495518	−5.932	−1.49251
52	H	0.142483	−2.63702	−4.01328
53	H	0.77485	−4.12228	−4.73844
54	H	−0.79529	−4.13637	−3.91376

Table S7 Optimized atom coordination of **q2P^{Hex}** based on a DFT calculation (RB3LYP/6-31G+(d)).

Tag	Symbol	X	Y	Z
1	C	4.258442	0.347794	1.097136
2	C	4.688549	1.646957	0.661434
3	S	3.369922	2.513978	−0.1338462
4	C	2.257669	1.143422	0.106432
5	C	2.946598	0.071654	0.774232
6	O	5.105082	−0.4673016	1.763219
7	O	2.290545	−1.0821842	1.02746
8	C	4.503514	−1.3049061	2.781861
9	C	3.077989	−2.3043885	0.952139
10	C	3.901122	−2.6097156	2.221866
11	C	0.265264	2.206963	−0.9949893
12	C	0.954019	1.135299	−0.3271161
13	S	−0.158097	−0.2356008	−0.0874017
14	C	−1.4764154	0.631343	−0.8830196
15	C	−1.0467344	1.931006	−1.3178583
16	O	0.921134	3.361276	−1.2477795

17	O	−1.8949663	2.74519	−1.9828349
18	C	0.131446	4.580604	−1.1718687
19	C	−1.2984256	3.587754	−3.0010021
20	C	−0.7042248	4.890851	−2.4347305
21	C	−2.7230481	0.049907	−1.0491211
22	C	5.935137	2.228624	0.826387
23	C	−3.8257138	0.697293	−1.6829758
24	N	−4.7671798	1.162932	−2.187806
25	C	−2.9563236	−1.2738506	−0.5691643
26	N	−3.1163607	−2.3559596	−0.1655573
27	C	6.167752	3.551984	0.344903
28	N	6.327246	4.633658	−0.0600678
29	C	7.038445	1.582131	1.459976
30	N	7.980748	1.117597	1.964218
31	C	5.078482	−3.5489004	1.823114
32	C	4.729932	−4.8336281	1.051517
33	C	5.968221	−5.7032013	0.783359
34	C	5.655055	−6.986629	0.002329
35	C	6.889388	−7.8601073	−0.2620346
36	C	6.567916	−9.1397676	−1.0431298
37	C	3.048014	−3.2713586	3.340309
38	C	1.718915	−2.6012239	3.730388
39	C	1.005939	−3.3516279	4.865825
40	C	−0.3333811	−2.7188629	5.26806
41	C	−1.0494065	−3.4682943	6.400229
42	C	−2.3855483	−2.829229	6.797082
43	C	−1.8363898	5.8442	−1.948986
44	C	−2.7172883	6.50062	−3.0235365
45	C	−3.8508772	7.337856	−2.4110273
46	C	−4.7421377	8.015864	−3.4605091
47	C	−5.8769382	8.851911	−2.8526941
48	C	−6.7631636	9.525049	−3.9074884
49	C	0.151615	5.577936	−3.5347042
50	C	1.494702	4.928795	−3.9125909
51	C	2.215711	5.70295	−5.0267825
52	C	3.568553	5.091578	−5.4166297
53	C	4.292079	5.86376	−6.5285617
54	C	5.641525	5.245613	−6.9133469

55	H	3.759655	−0.706014	3.316342
56	H	5.324143	−1.5329329	3.466812
57	H	2.340119	−3.0859279	0.761165
58	H	3.728198	−2.2192308	0.074621
59	H	0.865852	5.369014	−0.9907509
60	H	−0.5126969	4.498267	−0.2895546
61	H	−0.5456819	2.996796	−3.5321539
62	H	−2.1169311	3.80118	−3.6908339
63	H	5.606336	−3.8262627	2.747032
64	H	5.793655	−2.9651966	1.227201
65	H	4.260576	−4.5863189	0.088418
66	H	3.994095	−5.429716	1.608157
67	H	6.438627	−5.966643	1.742593
68	H	6.713793	−5.1127968	0.230097
69	H	5.18661	−6.7231231	−0.9584163
70	H	4.907012	−7.5758098	0.554738
71	H	7.357324	−8.1249387	0.697346
72	H	7.636996	−7.2722979	−0.8142687
73	H	7.469286	−9.7400832	−1.2149872
74	H	6.130742	−8.9075053	−2.0228156
75	H	5.84892	−9.7664551	−0.499828
76	H	2.830041	−4.3032906	3.037042
77	H	3.681459	−3.3555468	4.236787
78	H	1.883212	−1.5607427	4.042221
79	H	1.051358	−2.5531292	2.860527
80	H	0.835893	−4.3951384	4.560017
81	H	1.666546	−3.3950712	5.745257
82	H	−0.1646981	−1.6752739	5.575547
83	H	−0.9935381	−2.675344	4.388946
84	H	−1.2201668	−4.510143	6.092255
85	H	−0.3896226	−3.5133547	7.27923
86	H	−2.871269	−3.3882424	7.605846
87	H	−2.2443157	−1.7972363	7.143623
88	H	−3.079528	−2.8015754	5.947393
89	H	−2.4814003	5.280322	−1.2609031
90	H	−1.3729548	6.642628	−1.3487717
91	H	−3.1597223	5.73407	−3.6752703
92	H	−2.109011	7.145535	−3.6710713

93	H	−3.4189797	8.10548	−1.750875
94	H	−4.4707314	6.694447	−1.7692894
95	H	−5.1732003	7.248339	−4.1211572
96	H	−4.1227543	8.660124	−4.103391
97	H	−5.447456	9.619292	−2.1920243
98	H	−6.496455	8.208248	−2.211518
99	H	−7.5626685	10.11327	−3.4413761
100	H	−7.2353933	8.781057	−4.5618369
101	H	−6.1786465	10.20244	−4.543502
102	H	−0.4602257	5.668724	−4.443002
103	H	0.34618	6.609368	−3.2053913
104	H	2.1512	4.874244	−3.0349871
105	H	1.344494	3.891321	−4.24167
106	H	1.56821	5.750703	−5.9156827
107	H	2.368497	6.744104	−4.7042271
108	H	4.216098	5.044868	−4.5283806
109	H	3.417183	4.049997	−5.7395794
110	H	3.644829	5.912137	−7.4166702
111	H	4.445759	6.90357	−6.2050802
112	H	6.132341	5.820476	−7.7077992
113	H	6.323163	5.215467	−6.0538282
114	H	5.517822	4.216464	−7.2747387

Table S8 Optimized atom coordination of **q3P** based on a DFT calculation (RB3LYP/6-31G+(d)).

Tag	Symbol	X	Y	Z
1	C	4.123863	−0.54818	−0.43542
2	C	3.735648	1.940447	−0.64242
3	O	2.839069	−1.02702	−0.88955
4	O	2.377931	1.928543	−1.13524
5	C	1.720565	−0.34855	−0.53677
6	C	0.574231	−1.08446	−0.08417
7	S	−0.79094	0.020198	0.189436
8	C	0.181945	1.426726	−0.29423
9	C	1.508611	1.009545	−0.64985
10	C	−0.38248	−4.55968	0.715879
11	C	0.948923	−4.94443	0.3472
12	S	1.895558	−3.54231	−0.14568
13	C	0.513068	−2.45019	0.11392

14	C	−0.61617	−3.20487	0.576573
15	O	−1.22007	−5.47696	1.252946
16	O	−1.75373	−2.54757	0.906903
17	C	−2.56955	−5.55731	0.763779
18	C	−3.02113	−3.08688	0.470942
19	C	−3.4694	−4.37906	1.174781
20	C	−4.89131	−4.69467	0.662644
21	C	−3.4834	−4.20037	2.703011
22	C	−1.61293	3.163822	0.038606
23	C	−0.29545	2.722722	−0.31977
24	S	0.69813	4.125484	−0.78486
25	C	−0.6423	5.234836	−0.5062
26	C	−1.80479	4.529354	−0.0507
27	O	−2.50739	2.255222	0.49653
28	O	−2.89682	5.223139	0.346306
29	C	−3.86453	2.305252	0.003607
30	C	−4.19151	4.809266	−0.12224
31	C	−4.70465	3.496559	0.494474
32	C	−6.13877	3.277755	−0.03387
33	C	−4.71133	3.572749	2.031298
34	C	4.601853	0.754521	−1.0974
35	C	4.608286	0.627998	−2.631
36	C	6.032157	1.020889	−0.57921
37	C	−0.50854	6.601835	−0.72048
38	C	1.495514	−6.22257	0.353355
39	C	2.861833	−6.40892	−0.00824
40	N	3.983192	−6.52652	−0.30754
41	C	0.757592	−7.39881	0.678562
42	N	0.209396	−8.40079	0.913227
43	C	−1.57657	7.535526	−0.57435
44	N	−2.4085	8.34847	−0.49335
45	C	0.746949	7.1324	−1.13827
46	N	1.788054	7.534239	−1.47809
47	H	4.083899	−0.43702	0.657202
48	H	4.803078	−1.36861	−0.67932
49	H	4.140784	2.877286	−1.03247
50	H	3.70377	2.000084	0.454475
51	H	−2.54182	−5.65966	−0.3306

52	H	−2.94494	−6.49056	1.190595
53	H	−3.72699	−2.27986	0.684091
54	H	−2.97421	−3.2361	−0.61697
55	H	−5.58719	−3.88875	0.923866
56	H	−5.26875	−5.61733	1.117762
57	H	−4.91687	−4.82353	−0.42692
58	H	−2.48763	−3.97765	3.095187
59	H	−4.15257	−3.37976	2.989145
60	H	−3.8411	−5.11404	3.19197
61	H	−4.29893	1.367883	0.360803
62	H	−3.83131	2.282463	−1.09473
63	H	−4.84488	5.640718	0.153153
64	H	−4.16203	4.736176	−1.21891
65	H	−6.79191	4.103044	0.271411
66	H	−6.56544	2.352001	0.369748
67	H	−6.16842	3.214313	−1.1291
68	H	−3.70749	3.729417	2.434683
69	H	−5.34363	4.401472	2.370737
70	H	−5.10946	2.645697	2.461581
71	H	4.985732	1.549226	−3.09023
72	H	5.258294	−0.19717	−2.94501
73	H	3.607513	0.43879	−3.02833
74	H	6.062816	1.11643	0.513553
75	H	6.705024	0.204265	−0.86446
76	H	6.433063	1.945802	−1.00909

Table S9 Optimized atom coordination of **q4P** based on a DFT calculation (RB3LYP/6-31G+(d)).

Tag	Symbol	X	Y	Z
1	C	0.296712	−5.9126	−3.97853
2	C	1.59179	−5.51822	−3.51649
3	C	1.571091	−4.36698	−2.7475
4	C	0.270139	−3.80812	−2.54784
5	S	−0.94084	−4.80565	−3.38926
6	C	−0.02878	−7.00484	−4.78043
7	O	2.663997	−6.31443	−3.74662
8	C	3.865853	−5.71881	−4.26155
9	C	−0.05358	−2.68849	−1.79761
10	S	1.137155	−1.69782	−0.93194

11	C	−0.12678	−0.60147	−0.32788
12	C	−1.40554	−1.02757	−0.80343
13	C	−1.36632	−2.15561	−1.60189
14	C	0.131164	0.50221	0.473428
15	O	−2.50619	−0.28213	−0.52427
16	C	−3.69262	−0.95465	−0.05526
17	C	1.409932	0.928326	0.948951
18	C	1.370717	2.056393	1.747371
19	C	0.057969	2.589276	1.943082
20	S	−1.13277	1.598577	1.077463
21	O	2.510575	0.182885	0.669794
22	C	3.697004	0.855388	0.200771
23	C	−0.26574	3.70895	2.693257
24	S	0.945236	4.706524	3.534609
25	C	−0.29231	5.813508	4.12383
26	C	−1.58739	5.419097	3.661822
27	C	−1.56669	4.267811	2.892902
28	O	−2.65961	6.215302	3.89192
29	C	−3.86144	5.619693	4.406925
30	C	4.638452	−4.86136	−3.24365
31	C	3.844997	−3.59038	−2.89403
32	O	2.637729	−3.80063	−2.12994
33	C	−4.44206	−1.77832	−1.11665
34	C	−3.61746	−3.01032	−1.52515
35	O	−2.41494	−2.71176	−2.26188
36	C	4.446451	1.679088	1.262137
37	C	3.621854	2.911104	1.670602
38	O	2.419331	2.612569	2.407346
39	C	−4.63405	4.762175	3.389101
40	C	−3.84058	3.491189	3.039524
41	O	−2.63334	3.701434	2.275378
42	C	0.033185	6.90579	4.925672
43	C	4.968284	−5.67149	−1.97779
44	C	5.93966	−4.39907	−3.93369
45	C	−5.7329	−2.3012	−0.45027
46	C	−4.78966	−0.91525	−2.34218
47	C	4.794046	0.816045	2.487693
48	C	5.73729	2.201946	0.595744

49	C	−5.93523	4.299893	4.07921
50	C	−4.96394	5.572228	2.123207
51	C	−0.93318	7.79022	5.486742
52	N	−1.67272	8.537448	5.992049
53	C	1.39658	7.164956	5.246615
54	N	2.523334	7.349541	5.488314
55	C	−1.39217	−7.26398	−5.1014
56	N	−2.51893	−7.44856	−5.3431
57	C	0.937583	−7.88924	−5.34155
58	N	1.677122	−8.63644	−5.8469
59	H	4.469265	−6.57514	−4.57308
60	H	3.613149	−5.12684	−5.15307
61	H	−4.32734	−0.13885	0.301076
62	H	−3.41802	−1.58658	0.801293
63	H	4.331723	0.039582	−0.15555
64	H	3.422399	1.487303	−0.6558
65	H	−4.46485	6.476033	4.718422
66	H	−3.60869	5.027782	5.298478
67	H	4.444466	−2.94101	−2.2503
68	H	3.582489	−3.03647	−3.80641
69	H	−4.19195	−3.63993	−2.20932
70	H	−3.34689	−3.60669	−0.64236
71	H	4.196348	3.540726	2.354758
72	H	3.351291	3.507454	0.787803
73	H	−4.44006	2.841772	2.395846
74	H	−3.57803	2.93733	3.951916
75	H	5.545932	−5.06391	−1.27033
76	H	5.567159	−6.55367	−2.23294
77	H	4.063586	−6.01514	−1.46955
78	H	5.738537	−3.81286	−4.83946
79	H	6.54102	−3.78008	−3.25735
80	H	6.550458	−5.262	−4.22235
81	H	−6.31278	−2.90901	−1.15407
82	H	−6.36966	−1.46785	−0.13114
83	H	−5.51949	−2.91959	0.430891
84	H	−3.89303	−0.53053	−2.83508
85	H	−5.35419	−1.50152	−3.07678
86	H	−5.40792	−0.05894	−2.04666

87	H	5.358572	1.40233	3.22228
88	H	5.412303	−0.04027	2.192186
89	H	3.897413	0.431337	2.980594
90	H	5.523877	2.820316	−0.28543
91	H	6.317178	2.809759	1.299529
92	H	6.374046	1.36858	0.276631
93	H	−6.5366	3.680853	3.402929
94	H	−6.54603	5.162828	4.367846
95	H	−5.73406	3.713739	4.985008
96	H	−4.05927	5.915858	1.61492
97	H	−5.54161	4.964598	1.415806
98	H	−5.56282	6.454415	2.378331

Table S10 Optimized atom coordination of **q5P** based on a DFT calculation (RB3LYP/6-31G+(d)).

Tag	Symbol	X	Y	Z
1	C	−2.12148	−2.71103	−4.25757
2	C	−0.7473	−2.63087	−4.63085
3	C	0.044582	−1.93496	−3.7311
4	C	−0.65885	−1.43511	−2.59805
5	S	−2.37737	−1.87495	−2.71482
6	C	−3.13183	−3.34384	−4.97206
7	O	−0.31275	−3.29269	−5.73592
8	C	0.509734	−2.58402	−6.68314
9	C	−0.11784	−0.71958	−1.5317
10	S	1.597532	−0.27638	−1.41571
11	C	1.343273	0.559754	0.12977
12	C	−0.02738	0.470221	0.504928
13	C	−0.82013	−0.22387	−0.39663
14	C	2.358088	1.206297	0.832547
15	O	−0.46803	1.115345	1.619499
16	C	−1.27995	0.381079	2.554326
17	C	3.729513	1.294138	0.45832
18	C	4.522088	1.986303	1.360389
19	C	3.815239	2.486329	2.493697
20	S	2.101951	2.043414	2.379793
21	O	4.1669	0.653608	−0.65825
22	C	5.006142	1.379152	−1.57907
23	C	4.358788	3.212044	3.547122

24	S	6.075883	3.671433	3.632341
25	C	5.834485	4.521146	5.156818
26	C	4.466301	4.454853	5.559403
27	C	3.670984	3.73178	4.683234
28	O	4.03712	5.159402	6.636374
29	C	3.241276	4.483618	7.622226
30	C	1.947518	−2.31532	−6.20732
31	C	1.953877	−1.30126	−5.05013
32	O	1.392805	−1.77953	−3.81117
33	C	−2.71971	0.106561	2.086083
34	C	−2.72541	−0.88573	0.910139
35	O	−2.17035	−0.37559	−0.31622
36	C	6.444354	1.632953	−1.09469
37	C	6.45269	2.631038	0.075616
38	O	5.872336	2.129756	1.295324
39	C	1.800024	4.179269	7.17564
40	C	1.790967	3.124588	6.054959
41	O	2.328131	3.559192	4.787773
42	C	6.893537	5.150229	5.813949
43	C	2.645931	−3.62377	−5.79782
44	C	2.697342	−1.6577	−7.38565
45	C	−3.45356	−0.57806	3.258738
46	C	−3.43297	1.415424	1.704731
47	C	7.133951	0.315294	−0.70004
48	C	7.200984	2.300848	−2.26284
49	C	1.071177	3.553812	8.383934
50	C	1.079982	5.463387	6.728415
51	C	6.767899	5.785179	7.082721
52	N	6.735524	6.302339	8.128149
53	C	8.190333	5.148749	5.226729
54	N	9.240163	5.130718	4.716394
55	C	−4.51344	−3.42382	−4.62734
56	C	−5.3027	−4.0879	−5.55426
57	C	−4.56575	−4.58223	−6.67272
58	S	−2.86155	−4.15819	−6.53105
59	O	−4.95836	−2.80357	−3.50428
60	C	−5.84582	−3.5292	−2.62735
61	C	−7.27813	−3.73119	−3.15279

62	C	−7.28508	−4.70012	−4.3488
63	O	−6.6556	−4.18543	−5.53229
64	C	−5.04672	−5.30348	−7.76708
65	C	−8.08001	−4.40279	−2.01774
66	C	−7.92028	−2.3852	−3.53137
67	C	−4.15831	−5.67042	−8.81713
68	C	−6.39794	−5.73583	−7.89374
69	N	−7.48327	−6.13581	−8.04699
70	N	−3.40346	−5.9532	−9.66161
71	H	0.006643	−1.64352	−6.94904
72	H	0.518053	−3.23547	−7.56085
73	H	−0.76754	−0.55991	2.800863
74	H	−1.29225	1.015484	3.444989
75	H	5.019431	0.746046	−2.47055
76	H	4.509934	2.32773	−1.82909
77	H	3.238049	5.169789	8.473084
78	H	3.756651	3.559414	7.921384
79	H	2.983317	−1.04426	−4.78568
80	H	1.425512	−0.38171	−5.33955
81	H	−3.75456	−1.14307	0.644646
82	H	−2.19167	−1.80823	1.180085
83	H	5.935017	3.559971	−0.20262
84	H	7.48053	2.875139	0.356261
85	H	0.761386	2.84514	5.814636
86	H	2.335649	2.223207	6.369851
87	H	3.681415	−3.42836	−5.49348
88	H	2.668299	−4.32646	−6.63915
89	H	2.134657	−4.11191	−4.96406
90	H	2.224903	−0.71851	−7.70062
91	H	3.735534	−1.43736	−7.11074
92	H	2.720563	−2.32833	−8.25215
93	H	−4.4908	−0.8064	2.987179
94	H	−3.48001	0.07836	4.136334
95	H	−2.96863	−1.51697	3.555139
96	H	−2.93255	1.921713	0.875335
97	H	−4.46886	1.215945	1.404877
98	H	−3.45584	2.103846	2.558146
99	H	8.168888	0.501553	−0.38966

100	H	7.155885	−0.37715	−1.55038
101	H	6.617862	−0.1801	0.12644
102	H	6.731916	3.244129	−2.57053
103	H	8.236855	2.518554	−1.97882
104	H	7.230264	1.638293	−3.13585
105	H	0.031674	3.31329	8.130869
106	H	1.052374	4.253411	9.227374
107	H	1.558325	2.631263	8.724809
108	H	1.578009	5.929499	5.874316
109	H	0.043995	5.245067	6.440927
110	H	1.057153	6.194194	7.545447
111	H	−5.38229	−4.49757	−2.39121
112	H	−5.86421	−2.91937	−1.71978
113	H	−8.31107	−4.90564	−4.66486
114	H	−6.80622	−5.65222	−4.07774
115	H	−9.11348	−4.58727	−2.33255
116	H	−8.11468	−3.75902	−1.13072
117	H	−7.64369	−5.36497	−1.72034
118	H	−7.3728	−1.8885	−4.33655
119	H	−8.95302	−2.53455	−3.86794
120	H	−7.94064	−1.71032	−2.66668

15. References

S1 Y. Liand, B. Peng, J. Liang, Z. Tao and J. Chen, *Org. Lett.*, 2010, **12**, 1204−1207.

S2 C. Lin, T. Endo, M. Takase, M. Iyoda and T. Nishinaga, *J. Am. Chem. Soc.*, 2011, **133**, 11339–11350.

S3 B. D. Reeves, C. R. G. Grenier, A. A. Argun, A. Cirpan, T. D. McCarley and J. R. Reynolds, *Macromolecules*, 2004, **37**, 7559–7569.

S4 P. S. Chae, S. G. F. Rasmussen, R. R. Rana, K. Gotfryd, R. Chandra, M. A. Goren, A. C. Kruse, S. Nurva, C. J. Loland, Y. Pierre, D. Drew, J.-L. Popot, D. Picot, B. G. Fox, L. Guan, U. Gether, B. Byrne, B. Kobilka and S. H. Gellman, *Nat. Methods*, 2010, **7**, 1003−1008.

S5 V. Montano, M. M. B. Wempe, S. M. H. Does, J. C. Bijleveld, S. van der Zwaag and S. J. Garcia, *Macromolecules*, 2019, **52**, 8067−8078.

S6 G. S. Collier, R. Wilkins, A. L. Tomlinson and J. R. Reynolds, *Macromolecules*, 2021, **54**, 1677−1692.

S7 M. J. Frisch, G. W. Trucks, H. B. Schlegel, G. E. Scuseria, M. A. Robb, J. R. Cheeseman, G. Scalmani, V. Barone, G. A. Petersson, H. Nakatsuji, X. Li, M. Caricato, A. V. Marenich, J. Bloino, B. G. Janesko, R. Gomperts, B. Mennucci, H. P. Hratchian, J. V. Ortiz, A. F. Izmaylov, J. L. Sonnenberg, D. Williams-Young, F. Ding, F. Lipparini, F. Egidi, J. Goings, B. Peng, A. Petrone, T. Henderson, D. Ranasinghe, V. G. Zakrzewski, J. Gao, N. Rega, G. Zheng, W. Liang, M. Hada, M. Ehara, K. Toyota, R. Fukuda, J. Hasegawa, M. Ishida, T.

Nakajima, Y. Honda, O. Kitao, H. Nakai, T. Vreven, K. Throssell, J. A. Montgomery, Jr., J. E. Peralta, F. Ogliaro, M. J. Bearpark, J. J. Heyd, E. N. Brothers, K. N. Kudin, V. N. Staroverov, T. A. Keith, R. Kobayashi, J. Normand, K. Raghavachari, A. P. Rendell, J. C. Burant, S. S. Iyengar, J. Tomasi, M. Cossi, J. M. Millam, M. Klene, C. Adamo, R. Cammi, J. W. Ochterski, R. L. Martin, K. Morokuma, O. Farkas, J. B. Foresman and D. J. Fox, *Gaussian 16, Revision B.01*, Gaussian, Inc., Wallingford CT, 2016.

S8 P. R. Spackman, M. J. Turner, J. J. McKinnon, S. K. Wolff, D. J. Grimwood, D. Jayatilaka and M. A. Spackman, *J. Appl. Cryst.*, 2021, **54**, 1006–1011.